Probing wrong-sign Yukawa couplings at the LHC and a future linear collider

P. M. Ferreira[*] and Rui Santos[†]

Instituto Superior de Engenharia de Lisboa-ISEL, 1959-007 Lisboa, Portugal and Centro de Física Teórica e Computacional, Faculdade de Ciências, Universidade de Lisboa, Avenida Professor Gama Pinto 2, 1649-003 Lisboa, Portugal

John F. Gunion[‡]

Davis Institute for High Energy Physics, University of California, Davis, California 95616, USA

Howard E. Haber[§]

*Santa Cruz Institute for Particle Physics, University of California, Santa Cruz, California 95064, USA
and Ernest Orlando Lawrence Berkeley National Laboratory, University of California, Berkeley, California 94720, USA*

We consider the two-Higgs-doublet model as a framework in which to evaluate the viability of scenarios in which the sign of the coupling of the observed Higgs boson to down-type fermions (in particular, b-quark pairs) is opposite to that of the Standard Model (SM), while at the same time all other tree-level couplings are close to the SM values. We show that, whereas such a scenario is consistent with current LHC observations, both future running at the LHC and a future e^+e^- linear collider could determine the sign of the Higgs coupling to b-quark pairs. Discrimination is possible for two reasons. First, the interference between the b-quark and the t-quark loop contributions to the ggh coupling changes sign. Second, the charged-Higgs loop contribution to the $\gamma\gamma h$ coupling is large and fairly constant up to the largest charged-Higgs mass allowed by tree-level unitarity bounds when the b-quark Yukawa coupling has the opposite sign from that of the SM (the change in sign of the interference terms between the b-quark loop and the W and t loops having negligible impact).

I. INTRODUCTION

Now that the existence of a Higgs boson is firmly established [1,2], the ATLAS and CMS Collaborations at the Large Hadron Collider (LHC) have started probing the Higgs couplings to the fermions and to the gauge bosons [3–5]. With almost all data from the 8 TeV run analyzed, it becomes increasingly clear that the Standard Model (SM) predictions regarding the Higgs experimental rates are completely consistent with the current experimental data at the 95% C.L., in some cases at the 68% C.L. In the future, the LHC and an International Linear Collider (ILC) could further reinforce this consistency with ever higher precision or could eventually reveal some discrepancies. At this moment in time, it is important to delineate the portions of parameter space of models where qualitative and quantitative differences of the couplings with respect to the SM are consistent with current data but would be revealed by the upcoming LHC runs or at a future collider such as the ILC.

In this work, we will discuss the interesting possibility of a sign change in one of the Higgs Yukawa couplings, h_D for down-type fermions or h_U for up-type fermions, relative to the Higgs coupling to VV ($V = W^\pm$ or Z). It is well known that the current LHC results cannot differentiate between scenarios where a sign change occurs in the h_D Yukawa couplings (see e.g. Refs. [6–8]) simply using the measured properties of the observed Higgs-like boson and assuming no particles beyond those of the SM. For example, in the most recent fit of Ref. [8], it is found that while the coupling of the Higgs to top quarks must have the conventional positive sign relative to the Higgs coupling to VV, the couplings of down-type quarks and leptons are only constrained to $|h_D/h_D^{SM}| = 1.0 \pm 0.2$, where the sign ambiguity arises from the weak dependence of the gg and $\gamma\gamma$ loops on the Higgs couplings to bottom-quark pairs. The sign degeneracy in the determination of h_D at the LHC has also been stressed recently in Ref. [9].

In this paper, we will show that the sign of the bottom Yukawa can be determined with sufficient LHC data or at an ILC. The results of this paper will be established in the framework of the softly broken $\mathbb{Z}_2$-symmetric (CP-conserving) two-Higgs-doublet model (2HDM). The 2HDM possesses two limiting cases (called the decoupling

[*]ferreira@cii.fc.ul.pt
[†]rsantos@cii.fc.ul.pt
[‡]gunion@physics.ucdavis.edu
[§]haber@scipp.ucsc.edu

and alignment limits introduced in Sec. III), in which the Higgs couplings to VV, fermion pairs, and the cubic and quartic Higgs self-couplings approach their SM values. But, the 2HDM is also sufficiently flexible as to allow for a SM-like limit for the Higgs couplings to VV, up-type quark pairs and Higgs self-couplings, but with a coupling to down-type fermions that is opposite in sign to that of the SM. We can thus explore what happens in the context of this specific model when the only tree-level difference relative to the SM is the sign of h_D. The sign of h_D impacts both the ggh and $\gamma\gamma h$ couplings. The ggh coupling will change significantly when the sign of h_D is changed due to the fact that the sign of the interference between the bottom-quark and top-quark loops is reversed. The $h \to \gamma\gamma$ amplitude is altered primarily because the decoupling of the charged-Higgs loop contribution can be temporarily avoided until a rather large charged-Higgs mass, the boundary being set by the point at which the theory violates tree-level unitarity. Indeed, the nondecoupling of the charged-Higgs loop dominates over the change in the sign of interference terms involving the b-quark loop (whose interference is unobservably small on its own), and leads to a potentially observable decrease in the magnitude of the $\gamma\gamma h$ effective coupling. While the change in the sign of interference terms involving the bottom loop is a universal feature that can be used to resolve the relative sign of h_D versus h_U, the charged-Higgs temporary non-decoupling need not be. The latter proves essential in the $\gamma\gamma$ final state of Higgs decay to determine the sign of h_D relative to h_U, even allowing said discrimination at the next run of the LHC. Using the gg coupling is more generically useful and allows the sign determination both at the LHC (albeit somewhat indirectly) and at a future linear collider.

As already implicit in the statements above, it is important to explore the h_D sign issue in the context of a model in which both signs of h_D are allowed and physically distinguishable. The CP-conserving 2HDM provides one such context. Sensitivity to the sign of h_D requires that the measurable collider event rates depend significantly on it. The collider event rates are conveniently encoded in the cross section ratios μ_f^h defined by

$$\mu_f^h = \frac{\sigma \mathrm{BR}(h \to f)}{\sigma^{\mathrm{SM}} \mathrm{BR}(h_{\mathrm{SM}} \to f)} \qquad (1.1)$$

where σ is the Higgs production cross section and $\mathrm{BR}(h \to f)$ is the branching ratio of the decay to some given final state f; σ^{SM} and $\mathrm{BR}(h_{\mathrm{SM}} \to f)$ are the expected values for the same quantities in the SM. The experimentally measured values of μ_f^h for a variety of final states f at the LHC already provide interesting constraints on the 2HDM parameter space [10].

In this paper, we do not separate different LHC initial state production mechanisms ($gg \to h$, $VV \to h$, $b\bar{b} \to h$, Vh associated production and $t\bar{t}h$ associated production);

that is, we sum over all production mechanisms in computing the cross section. In our analysis of Higgs phenomena at the ILC, we consider only the $e^+e^- \to Zh$ production process. We employ the notation $\mu_f^h(\mathrm{LHC}, \mathrm{ILC})$ when discussing these ratios for the LHC and ILC, respectively. In deciding whether or not a given 2HDM parameter choice is excluded by LHC data for given values of $\mu_f^h(\mathrm{LHC})$, all the currently well-measured final states $f = WW^*, ZZ^*, b\bar{b}, \tau^+\tau^-, \gamma\gamma$ must be employed. In particular, we will find that $h_D < 0$ is only consistent with current LHC Higgs data for a 2HDM of type-II if the deviations in the $\gamma\gamma h$ and/or ggh couplings will be detectable in the future with the LHC operating at $\sqrt{s} \sim 14$ TeV, assuming an accumulation of luminosity $L \geq 300$ fb^{-1}, and at a future ILC.

This paper is organized as follows. In Sec. 2, we describe the 2HDM and the constraints imposed by theoretical and phenomenological considerations. In Sec. 3 we introduce the decoupling and alignment limits, and then define the wrong-sign Yukawa couplings scenario and discuss its properties. In Sec. 4 we analyze the detailed phenomenology of the wrong-sign Yukawa coupling scenario, and in Sec. 5, we exhibit the results of our analysis. Our conclusions are presented in Sec. 6. Appendix A provides details regarding the Higgs basis scalar potential parameters of the 2HDM relevant for Sec. 3. The Higgs sector of the minimal supersymmetric extension of the Standard Model (MSSM) [11] is a special case of the type-II 2HDM introduced in Sec. 2. The possibility of an MSSM Higgs sector with an opposite-sign $hb\bar{b}$ coupling relative to the SM is addressed in Appendix B. Finally, Appendix C explains the nondecoupling behavior of the charged-Higgs loop contribution to the $h \to \gamma\gamma$ amplitude in a type-II 2HDM that is particularly relevant when h_D has a sign opposite that of the SM.

II. MODELS AND CONSTRAINTS

The 2HDM is an extension of the scalar sector of the SM with an extra hypercharge-one scalar doublet field, first introduced in Ref. [12] as a means to explain matter-antimatter asymmetry (see Refs. [13,14] for a detailed description of the model). The most general Yukawa Lagrangian, in terms of the quark mass-eigenstate fields, is

$$-\mathcal{L}_Y = \bar{U}_L \tilde{\Phi}_a^0 \eta_a^U U_R + \bar{D}_L K^\dagger \tilde{\Phi}_a^- \eta_a^U U_R + \bar{U}_L K \Phi_a^+ \eta_a^{D\dagger} D_R$$
$$+ \bar{D}_L \Phi_a^0 \eta_a^{D\dagger} D_R + \mathrm{H.c.}, \qquad (2.1)$$

where $\tilde{\Phi}_a \equiv (\tilde{\Phi}^0, \tilde{\Phi}^-)^T = i\sigma_2 \Phi_a^*$ and K is the CKM mixing matrix. In Eq. (2.1) there is an implicit sum over the index $a = 1, 2$, and the $\eta^{U,D}$ are 3×3 Yukawa coupling matrices. In general, such models give rise to couplings corresponding to tree-level Higgs-mediated flavor-changing neutral currents (FCNCs), in clear disagreement with experimental data.

TABLE I. Couplings of the fermions to the lighter and heavier CP-even scalars (h and H), and the CP-odd scalar (A), relative to the corresponding SM value of m_f/v.

	Type-I			Type-II		
	h	A	H	h	A	H
Up-type quarks	$\cos\alpha/\sin\beta$	$\cot\beta$	$\sin\alpha/\sin\beta$	$\cos\alpha/\sin\beta$	$\cot\beta$	$\sin\alpha/\sin\beta$
Down-type quarks and charged leptons	$\cos\alpha/\sin\beta$	$-\cot\beta$	$\sin\alpha/\sin\beta$	$-\sin\alpha/\cos\beta$	$\tan\beta$	$\cos\alpha/\cos\beta$

A natural way to avoid FCNC interactions is to impose a $\mathbb{Z}_2$ symmetry on the dimension-four terms of the Higgs Lagrangian in order to set two of the η_a^Q equal to zero in Eq. (2.1) [15]. This in turn implies that one of the two Higgs fields is odd under the $\mathbb{Z}_2$ symmetry. The Higgs potential can thus be written as

$$\mathcal{V} = m_{11}^2 \Phi_1^\dagger \Phi_1 + m_{22}^2 \Phi_2^\dagger \Phi_2 - (m_{12}^2 \Phi_1^\dagger \Phi_2 + \text{H.c.})$$
$$+ \frac{1}{2}\lambda_1(\Phi_1^\dagger\Phi_1)^2 + \frac{1}{2}\lambda_2(\Phi_2^\dagger\Phi_2)^2 + \lambda_3\Phi_1^\dagger\Phi_1\Phi_2^\dagger\Phi_2$$
$$+ \lambda_4\Phi_1^\dagger\Phi_2\Phi_2^\dagger\Phi_1 + \left[\frac{1}{2}\lambda_5(\Phi_1^\dagger\Phi_2)^2 + \text{H.c.}\right], \quad (2.2)$$

where m_{12}^2 softly breaks the $\mathbb{Z}_2$ symmetry. In particular, we do not allow a hard breaking of the $\mathbb{Z}_2$ symmetry, which implies that the term of the form $(\Phi_1^\dagger\Phi_2)(\lambda_6\Phi_1^\dagger\Phi_1 + \lambda_7\Phi_2^\dagger\Phi_2) + \text{H.c.}$ is absent. For simplicity we will work with a CP-conserving scalar potential by choosing m_{12}^2 and λ_5 to be real.

The 2HDM parameters are chosen such that electric charge is conserved while neutral Higgs fields acquire real vacuum expectation values,[1] $\langle\Phi_a^0\rangle = v_a/\sqrt{2}$ (for $a = 1, 2$), where

$$v^2 \equiv v_1^2 + v_2^2 = \frac{4m_W^2}{g^2} = (246 \text{ GeV})^2, \quad \text{and} \quad \tan\beta \equiv \frac{v_2}{v_1}. \quad (2.3)$$

By convention, we take $0 \le \beta \le \frac{1}{2}\pi$ (after a suitable rephasing of the Higgs doublet fields). From the 8 degrees of freedom we end up with three Goldstone bosons, a charged-Higgs pair, two CP-even neutral Higgs states, h and H (defined such that $m_h \le m_H$), and one CP-odd neutral Higgs boson A. The CP-even Higgs squared-mass matrix is diagonalized by an angle α, which is defined modulo π. The coupling of h to VV is specified by

$$g_{hWW} = gm_W \sin(\beta - \alpha). \quad (2.4)$$

As noted above, Higgs-mediated tree-level FCNCs can be avoided by imposing a $\mathbb{Z}_2$ symmetry that is preserved by all dimension-four interactions of the Higgs Lagrangian. Different choices for the transformation of the fermion fields under this $\mathbb{Z}_2$ lead to different Higgs-fermion interactions. In this paper, we shall focus on two different choices, which lead to models that are called the type-I [18,19] and type-II [19,20] 2HDM. In the type-I 2HDM, $\eta_1^U = \eta_1^D = 0$ in Eq. (2.1), whereas in the type-II 2HDM, $\eta_1^U = \eta_2^D = 0$. In the former all fermions couple exclusively to Φ_2 while in the latter the up-type quarks couple exclusively to Φ_2 and the down-type quarks and charged leptons couple exclusively to Φ_1. In both the type-I and type-II 2HDM, the Higgs-fermion couplings are flavor diagonal and depend on the two angles α and β as shown in Table I. The tree-level MSSM Higgs sector is a special case of the type-II 2HDM [11].

The most relevant constraints on the 2HDM are briefly discussed in Ref. [21]. Here, we will just enumerate the constraints imposed on the parameters of the CP-conserving 2HDM.

(i) The Higgs potential is bounded from below [22].
(ii) Tree-level unitarity is imposed on the quartic Higgs couplings [23].
(iii) It complies with S and T parameters [24,25] as derived from electroweak precision observables [26–28].
(iv) The global minimum of the Higgs potential is unique [29] and no spontaneous charge or CP-breaking occurs [17].
(v) Indirect constraints on the $(m_{H^\pm}, \tan\beta)$ plane stem from loop processes involving charged-Higgs bosons. They originate mainly from B physics observables [27,30,31] and from the $R_b \equiv \Gamma(Z \to b\bar{b})/\Gamma(Z \to \text{hadrons})$ [27,32–36] measurement. In particular, for the type-II 2HDM, $m_{H^\pm} \gtrsim 340$ GeV is required.
(vi) LEP searches based on $e^+e^- \to H^+H^-$ [37] and recent LHC results [38,39] based on $pp \to \bar{t}t(\to H^+\bar{b})$ constrain the mass of the charged Higgs to be above $O(100)$ GeV, depending on the model type.

Finally we should note that there is an unexplained discrepancy between the value of $\bar{B} \to D^{(*)}\tau^-\bar{\nu}_\tau$ measured by the *BABAR* Collaboration [40] and the corresponding SM prediction. The observed deviation is of the order 3.4σ.

---

[1]A sufficient condition for guaranteeing that the vacuum is CP invariant is $\lambda_5|v_1||v_2| \le |m_{12}^2|$ (see e.g. Appendix B of Ref. [16]). Moreover, the existence of a tree-level scalar potential minimum that breaks the electroweak symmetry but preserves both the electric charge and CP symmetries, ensures that no additional tree-level potential minima that spontaneously break the electric charge and/or CP symmetry can exist [17]. As such, in our simulations we can be certain that v_1 and v_2 can be chosen real.

If confirmed, this observation would exclude both the SM and the version of the 2HDM considered in this work.

III. DECOUPLING, ALIGNMENT, DELAYED DECOUPLING AND THE WRONG-SIGN YUKAWA COUPLINGS

In light of the fact that the LHC Higgs data is consistent with the predictions of the Standard Model with one complex hypercharge-one Higgs doublet, it is of interest to consider the limit of the 2HDM in which the properties of the lightest *CP*-even Higgs boson *h* approach those of the SM Higgs boson. It is convenient in this section to adopt a sign convention in which $\sin(\beta - \alpha)$ is non-negative,[2] i.e. $0 \leq \beta - \alpha \leq \pi$. Since

$$\frac{g_{hVV}}{g_{h_{\text{SM}}VV}} = \sin(\beta - \alpha), \quad \text{where } V = W^{\pm} \text{ or } Z, \quad (3.1)$$

it follows that *h* is SM-like in the limit of $\cos(\beta - \alpha) \to 0$.

It is convenient to rewrite the Higgs potential of Eq. (2.2) in terms of new scalar doublet fields defined in the Higgs basis [41–47]. The coefficients of the quartic terms of the scalar potential in the Higgs basis are denoted by Z_i (where $i = 1, 2, \ldots, 7$). Expressions for the Z_i in terms of the λ_i defined by Eqs. (A6)–(A10) are given in Appendix A. In particular, using Eqs. (A6) and (A9), it follows that

$$\cos^2(\beta - \alpha) = \frac{Z_1 v^2 - m_h^2}{m_H^2 - m_h^2}, \quad (3.2)$$

$$\sin(\beta - \alpha)\cos(\beta - \alpha) = -\frac{Z_6 v^2}{m_H^2 - m_h^2}. \quad (3.3)$$

By assumption, the sizes of the scalar potential parameters (in any basis) are limited by tree-level unitarity constraints. This means that $Z_1/(4\pi) \lesssim \mathcal{O}(1)$ and $Z_6/(4\pi) \lesssim \mathcal{O}(1)$. It follows that if $m_H \gg v$ then $|\cos(\beta - \alpha)| \ll 1$ in which case *h* has SM-like couplings to *VV*. This is the *decoupling limit* [16,48], where $m_{H^\pm}^2 - m_A^2 \sim \mathcal{O}(v^2)$ and $m_H^2 - m_A^2 \sim \mathcal{O}(v^2)$ [i.e. $m_H \sim m_A \sim m_{H^\pm} \gg m_h$], and the *hVV* couplings approach those of the Standard Model. That is, below the common scale of the heavy Higgs states, the effective field theory that describes Higgs physics is the Standard Model with a single hypercharge-one Higgs doublet. However, note that if *h* is SM-like, it does not necessarily follow that the masses of *H*, *A* and $H^\pm$ are large. Indeed, Eq. (3.3) implies that it is possible to achieve $|\cos(\beta - \alpha)| \ll 1$ by taking $|Z_6| \ll 1$ [16,49]. The limit where $Z_6 \to 0$ is called the *alignment limit* [50–53], since in this limit the mixing

of the two-Higgs-doublet fields in the Higgs basis is suppressed.[3]

In both the decoupling and alignment limits, the couplings of *h* to the fermions should also approach their SM values. To see how this happens, consider the $h\bar{f}f$ couplings in the case of the type-II 2HDM. Using the results displayed in Table I, the $h\bar{f}f$ couplings relative to those of the SM (for $f = U, D$) are given by

$$h\bar{D}D: \quad -\frac{\sin\alpha}{\cos\beta} = \sin(\beta - \alpha) - \cos(\beta - \alpha)\tan\beta, \quad (3.4)$$

$$h\bar{U}U: \quad \frac{\cos\alpha}{\sin\beta} = \sin(\beta - \alpha) + \cos(\beta - \alpha)\cot\beta. \quad (3.5)$$

In the case of $\cos(\beta - \alpha) = 0$, the $h\bar{f}f$ couplings reduce precisely to the corresponding SM values. However, for values of $\cos(\beta - \alpha)$ that are small but nonzero, the decoupling limit can be "delayed" if either $\tan\beta$ or $\cot\beta$ is large. On the other hand, it is desirable to have $(m_t/v)\cot\beta \lesssim 1$ and $(m_b/v)\tan\beta \lesssim 1$, in order to avoid nonperturbative behavior in the couplings of *H*, *A* and $H^\pm$ to the third generation at scales far below the Planck scale. In addition, phenomenological constraints arising from *B* physics observables and R_b mentioned above rule out regions of $\tan\beta \lesssim 1$ for large regions of the 2HDM parameter space [31]. Consequently, we shall focus on the parameter region where

$$1 \lesssim \tan\beta \lesssim 50. \quad (3.6)$$

In this case, decoupling is not delayed for the coupling of *h* to up-type fermions. On the other hand, for $\tan\beta$ in the range of interest, it is certainly possible to have $\sin(\beta - \alpha)$ close to 1 and yet have significant departures from decoupling in the coupling of *h* to down-type fermions. That is, it is possible to have $\sin(\beta - \alpha)$ close to 1 and yet have $\cos(\beta - \alpha)\tan\beta \sim \mathcal{O}(1)$. Since $\cos(\beta - \alpha)$ behaves as v^2/m_H^2 in the decoupling limit [cf. Eq. (3.3)], we see that the $h\bar{D}D$ coupling approaches its SM value if

$$m_H^2 \gg v^2 \tan\beta. \quad (3.7)$$

Thus, if $\tan\beta \gg 1$ we say that we have *delayed decoupling* [54], since a much larger value of the heavy Higgs mass scale is required to achieve decoupling of the heavy Higgs states (i.e. $m_H \gg v$ is not sufficient).[4]

The *wrong-sign Yukawa coupling* regime is defined as the region of 2HDM parameter space in which at least one

---

[2]The implications of an alternative convention $|\alpha| \leq \frac{1}{2}\pi$, employed in the 2HDM parameter scans of Secs. IV and V, will be addressed later in this section.

[3]In the alignment limit where $Z_6 \to 0$, it is possible to have $\sin(\beta - \alpha) \to 0$, in which case we would identify the heavier *CP*-even state *H* as the SM-like Higgs boson. We will not consider this possibility further in this paper.

[4]Likewise, the alignment limit is also delayed, since the condition $|Z_6| \ll 1$ is now replaced by $|Z_6|\tan\beta \ll 1$.

of the couplings of h to down-type and up-type fermion pairs is *opposite* in sign to the corresponding coupling of h to VV. This is to be contrasted with the Standard Model, where the couplings of h to $\bar{f}f$ and VV are of the same sign. Note that in the convention where $\sin(\beta - \alpha) \geq 0$, the hVV couplings in the 2HDM are always non-negative. To analyze the wrong-sign coupling regime, it is more convenient to rewrite the type-II Higgs-fermion Yukawa couplings, given by Eqs. (3.4) and (3.5), in the following form:

$$h\bar{D}D: \quad -\frac{\sin\alpha}{\cos\beta} = -\sin(\beta + \alpha) + \cos(\beta + \alpha)\tan\beta, \quad (3.8)$$

$$h\bar{U}U: \quad \frac{\cos\alpha}{\sin\beta} = \sin(\beta + \alpha) + \cos(\beta + \alpha)\cot\beta. \quad (3.9)$$

In the case of $\sin(\beta + \alpha) = 1$, the $h\bar{D}D$ coupling normalized to its SM value is equal to -1 (whereas the normalized $h\bar{U}U$ coupling is $+1$). Note that in this limiting case, $\sin(\beta - \alpha) = -\cos 2\beta$, which implies that the wrong-sign $h\bar{D}D$ Yukawa coupling can only be achieved for values of $\tan\beta > 1$. Likewise, in the case of $\sin(\beta + \alpha) = -1$, the $h\bar{U}U$ coupling normalized to its SM value is equal to -1 (whereas the normalized $h\bar{D}D$ coupling is $+1$). In this limiting case, $\sin(\beta - \alpha) = \cos 2\beta$, which implies that the wrong-sign $h\bar{U}U$ couplings can only be achieved for $\tan\beta < 1$. In the type-I 2HDM, both the $h\bar{D}D$ and $h\bar{U}U$ couplings are given by Eq. (3.5) [or equivalently by Eq. (3.9)]. Thus, for $\sin(\beta - \alpha) = -1$, both the normalized $h\bar{D}D$ and $h\bar{U}U$ couplings are equal to -1, which is only possible if $\tan\beta < 1$. In light of Eq. (3.6), only the wrong-sign $h\bar{D}D$ coupling regime of the type-II 2HDM can be realistically achieved.

It should be emphasized that the above conclusions do not depend on the convention adopted for the range of the angle α. In the convention used in Secs. IV and V of this paper, we scan over $|\alpha| \leq \pi/2$, which allows for the possibility of negative $\sin(\beta - \alpha)$. However, the definition of the wrong-sign Yukawa coupling is not changed as it refers to the *relative* sign of the $h\bar{f}f$ and hVV couplings. To translate between both conventions, one simply must shift $\alpha \to \alpha \pm \pi$ (the sign chosen so that α is in its desired range). In practice, the scans of Secs. IV and V focus on the wrong-sign $h\bar{D}D$ coupling regime where $\tan\beta > 1$, in which case $\sin(\beta - \alpha) > 0$ and the distinction between the two conventions becomes moot.

In the above discussion of the wrong-sign Yukawa coupling regime, we have not yet imposed the requirement that h is SM-like. In particular, for a fixed value of $\tan\beta$, the limit of $\sin(\beta + \alpha) \to 1$ is *not* the decoupling limit (indeed the hVV couplings do not approach their SM values except in the limit of $\alpha \to 0$ and $\beta \to \frac{1}{2}\pi$). This implies that for $|\cos(\beta - \alpha)| \ll 1$ we must have $\tan\beta \gg 1$, Likewise, the limit of $\sin(\beta + \alpha) = -1$ is not the decoupling limit unless $\beta \to 0$ and $\alpha \to -\frac{1}{2}\pi$, i.e. $\cot\beta \gg 1$. Again, we see that for values of $\tan\beta > 1$, among all possible wrong-sign Yukawa coupling scenarios only the wrong-sign $h\bar{D}D$ coupling in the type-II 2HDM is phenomenologically viable.

Therefore, in this paper, we shall explore the possibility that the $h\bar{D}D$ coupling normalized to its SM value is close to -1 in the type-II 2HDM.[5] This scenario was first examined in Ref. [55] and then later clarified in Ref. [16]. Current LHC Higgs observations are not sufficiently precise as to allow one to distinguish this case from that of the SM Higgs boson. To study this case, we first define a parameter ϵ by defining the normalized $h\bar{D}D$ coupling to be given by

$$-\frac{\sin\alpha}{\cos\beta} = -1 + \epsilon. \quad (3.10)$$

Multiplying Eq. (3.10) by $-2\cos^2\beta$, and employing the trigonometric identity, $2\cos\beta\sin\alpha = \sin(\beta + \alpha) - \sin(\beta - \alpha)$, it follows that[6]

$$\sin(\beta + \alpha) - \sin(\beta - \alpha) = 2(1 - \epsilon)\cos^2\beta. \quad (3.11)$$

By employing the trigonometric identity $\sin(\beta - \alpha) = \sin 2\beta\cos(\beta + \alpha) - \cos 2\beta\sin(\beta + \alpha)$ and taking $0 \leq \beta \leq \frac{1}{2}\pi$, one can also derive

$$\sin(\beta + \alpha) = (1 - \epsilon)\cos^2\beta + \sin\beta\sqrt{1 - (1 - \epsilon)^2\cos^2\beta}, \quad (3.12)$$

$$\cos(\beta + \alpha) = -(1 - \epsilon)\sin\beta\cos\beta + \cos\beta\sqrt{1 - (1 - \epsilon)^2\cos^2\beta}. \quad (3.13)$$

Using Eqs. (3.4) and (3.10), it follows that

$$\tan\beta = \frac{1 + \sin(\beta - \alpha) - \epsilon}{\cos(\beta - \alpha)}. \tag{3.14}$$

Since the hVV couplings are assumed to be close to the SM, we still must impose the constraint that $|\cos(\beta - \alpha)| \ll 1$. Thus, in the case of the wrong-sign $h\bar{D}D$ Yukawa coupling, we must have $\tan\beta \gg 1$, which is the region of delayed decoupling defined below Eq. (3.7).

For completeness, we also also examine the case of a wrong-sign $h\bar{U}U$ coupling in the type-II 2HDM (or the case of the wrong-sign $h\bar{U}U$ and $h\bar{D}D$ couplings in the type-I 2HDM) by taking $\sin(\beta + \alpha)$ close to -1

[cf. Eq. (3.9)]. To study this case, we first define a parameter ϵ' via

$$\frac{\cos\alpha}{\sin\beta} = -1 + \epsilon', \tag{3.15}$$

which yields an $h\bar{U}U$ coupling normalized to its SM value given by $-1 + \epsilon'$. An analysis similar to the one used in the case of the wrong-sign $h\bar{D}D$ Yukawa coupling yields

$$\sin(\beta + \alpha) + \sin(\beta - \alpha) = -2(1 - \epsilon')\sin^2\beta, \tag{3.16}$$

and

$$\sin(\beta + \alpha) = -(1 - \epsilon')\sin^2\beta - \cos\beta\sqrt{1 - (1 - \epsilon')^2\sin^2\beta}, \tag{3.17}$$

$$\cos(\beta + \alpha) = -(1 - \epsilon')\sin\beta\cos\beta + \sin\beta\sqrt{1 - (1 - \epsilon')^2\sin^2\beta}. \tag{3.18}$$

Using Eqs. (3.5) and (3.14), it follows that

$$\cot\beta = \frac{-\sin(\beta - \alpha) - 1 + \epsilon'}{\cos(\beta - \alpha)}. \tag{3.19}$$

For values of $|\cos(\beta - \alpha)| \ll 1$, Eq. (3.19) can only be satisfied if $\cot\beta \gg 1$, which lies outside the range of $\tan\beta$ under consideration [cf. Eq. (3.6)], as previously noted.

To complete the analysis of the tree-level Higgs couplings, we briefly look at the h self-coupling. In the 2HDM, the hhh coupling[7] is given by [16]

$$G_{hhh} = -3v[Z_1\sin^3(\beta - \alpha) + 3Z_6\cos(\beta - \alpha)\sin^2(\beta - \alpha)$$
$$+ (Z_3 + Z_4 + Z_5)\sin(\beta - \alpha)\cos^2(\beta - \alpha)$$
$$+ Z_7\cos^3(\beta - \alpha)], \tag{3.20}$$

where in the softly broken $\mathbb{Z}_2$-symmetric 2HDM, the Z_i are given in Eqs. (A6) and (A10). Rewriting the Z_i in terms of the λ_i yields

$$G_{hhh} = 3v[-\cos\beta\sin^2\alpha\lambda_1 + \sin\beta\cos^3\alpha\lambda_2$$
$$- \sin\alpha\cos\alpha\cos(\beta + \alpha)(\lambda_3 + \lambda_4 + \lambda_5)], \tag{3.21}$$

which reproduces the result given in Ref. [56]. Using the results of Appendix D of Ref. [16], we can rewrite the hhh coupling in a more convenient form,

---

[7]A similar analysis can be given for the $hhhh$ coupling using the results given in Ref. [16]. However, this coupling cannot be realistically probed by the LHC and ILC, so we will not provide the explicit expressions here.

$$G_{hhh} = \frac{-3}{v\sin^2\beta\cos^2\beta}[\sin\beta\cos\beta(\cos\beta\cos^3\alpha - \sin\beta\sin^3\alpha)m_h^2$$
$$- \cos^2(\beta - \alpha)\cos(\beta + \alpha)m_{12}^2], \tag{3.22}$$

which reproduces the result given in Ref. [57] (after correcting a missing factor of 2).

In the decoupling/alignment limit where $\sin(\beta - \alpha) = 1$, we have $\cos\alpha = \sin\beta$ and $\sin\alpha = -\cos\beta$. Then, the hhh coupling reduces to the SM value,

$$G_{hhh} \to G_{hhh}^{SM} = -\frac{3m_h^2}{v}. \tag{3.23}$$

In the wrong-sign Yukawa coupling limit for type-II Higgs couplings to down-type [up-type] fermions, respectively, where $\sin(\beta + \alpha) = +1$ [-1], we have $\cos\alpha = +[-]\sin\beta$ and $\sin\alpha = +[-]\cos\beta$, so that

$$G_{hhh} \to -[+]G_{hhh}^{SM}\cos 2\beta, \tag{3.24}$$

which reduces to the SM value only when $\beta \to \frac{1}{2}\pi$ [$\beta \to 0$] for type-II Higgs couplings to down-type [up-type] fermions, respectively. It is quite remarkable that this matches the behavior of the hVV coupling in the same limit. In particular, for $\sin(\beta + \alpha) = \pm 1$, we have $\sin(\beta - \alpha) = \mp\cos 2\beta$, as previously noted. Hence in the wrong-sign Yukawa coupling limit, Eq. (3.1) yields

$$G_{hVV} \to -[+]G_{hVV}^{SM}\cos 2\beta. \tag{3.25}$$

Of course, the corresponding first order corrections to the hhh and hVV couplings will differ as one moves away from the strict limiting case treated above.

In the decoupling and alignment limits discussed at the beginning of this subsection, the tree-level couplings of h

approach the corresponding values of the SM Higgs boson. The behavior of the decoupling and alignment limits differ when one-loop effects are taken into account. In the decoupling limit, the properties of h continue to mimic those of the SM-like Higgs boson since the effects of the H, A and $H^\pm$ loops decouple in the limit of heavy scalar masses. In contrast, the alignment limit only requires that $|Z_6| \ll 1$, so that in principle the masses of H, A and $H^\pm$ could be relatively close to the electroweak scale. In this case, the loop effects mediated by H, A and $H^\pm$ can compete with other electroweak radiative effects and thus distinguish between h and the SM Higgs boson.

In processes in which the one-loop effects are small corrections to tree-level results, very precise measurements will be required to distinguish between h and the SM Higgs boson in the alignment limit. Indeed, a much more fruitful experimental approach in this case is to search directly for the H, A and $H^\pm$ scalars. However, in Higgs processes that are absent at tree level but arise at one-loop, the loop effects mediated by H, A or $H^\pm$ can compete directly with deviations that arise due to small departures from the alignment limit. The most prominent example is the decay rate for $h \to \gamma\gamma$. Departures from the SM decay rate for $h \to \gamma\gamma$ can arise either from deviations in the hW^+W^-, $h\bar{t}t$ and/or $h\bar{b}b$ couplings from their SM values, or from the contributions of the charged-Higgs boson loop (which is not present in the SM). To compute the latter, we need to compute the hH^+H^- coupling. Using the results of Ref. [16],

$$G_{hH^+H^-} = -v[Z_3 \sin(\beta - \alpha) + Z_7 \cos(\beta - \alpha)], \quad (3.26)$$

where Z_3 and Z_7 are defined in terms of the λ_i in Eqs. (A8) and (A10). It is convenient to reexpress the hH^+H^- coupling in terms of the Higgs masses and λ_5. Using the expressions given in Appendix D of Ref. [16], we obtain

$$G_{hH^+H^-} = \frac{1}{v}[(2m_A^2 - 2m_{H^\pm}^2 - m_h^2 + 2\lambda_5 v^2)\sin(\beta - \alpha)$$
$$+ (m_A^2 - m_h^2 + \lambda_5 v^2)(\cot\beta - \tan\beta)\cos(\beta - \alpha)],$$
$$(3.27)$$

where

$$m_A^2 - m_{H^\pm}^2 = \frac{1}{2}v^2(\lambda_4 - \lambda_5). \quad (3.28)$$

In the alignment limit where the masses of H, A and $H^\pm$ are of order the electroweak scale, $G_{hH^+H^-} \sim \mathcal{O}(v)$ and the charged-Higgs loops can compete with the SM loops that contribute to the $h \to \gamma\gamma$ one-loop amplitude. In the normal decoupling limit where $m_{H^\pm}^2 \sim m_A^2 \gg \mathcal{O}(v^2)$ and $|\cos(\beta - \alpha)| \sim v^2/m_A^2$, $G_{hH^+H^-} \sim \mathcal{O}(v)$ as expected, in which case the charged-Higgs loop contribution to the $h \to \gamma\gamma$ amplitude is suppressed by a factor of $v^2/m_{H^\pm}^2$. Note that this factor is of the same order as $\cos(\beta - \alpha)$. The

contribution of the fermion loops also deviates from the SM by a factor of $\mathcal{O}(\cos(\beta - \alpha))$ due to the modified tree-level $h\bar{f}f$ couplings [cf. Eqs. (3.4) and (3.5)].[8] However, in the decoupling limit the contribution of the bottom-quark loop is suppressed by a factor of m_b^2/v^2 and can thus be ignored. We conclude that the deviation from the SM in the decoupling limit is due primarily to the top-quark loop and the charged-Higgs loop, whose contributions to the $h \to \gamma\gamma$ decay amplitude are of the same order of magnitude.

The form of the hH^+H^- coupling given in Eq. (3.27) suggests the existence of 2HDM parameter regimes in which $G_{hH^+H^-} \gg \mathcal{O}(v)$, even under the assumption that $\cos(\beta - \alpha) \sim \mathcal{O}(v^2/m_H^2) \ll 1$. For example, if we allow $\lambda_4 - \lambda_5$ to be large and if $m_{H^\pm}$, m_A, $m_H \gg v$, then it possible to have $m_A^2 - m_{H^\pm}^2 \sim \mathcal{O}(m_{H^\pm}^2)$. It would then follow that the contribution of the charged-Higgs loop contribution to the $h \to \gamma\gamma$ amplitude, which scales as $G_{hH^+H^-}/m_{H^\pm}^2$, approaches a constant in the region of $m_{H^\pm} \gg m_h$. This nondecoupling behavior was first emphasized in Ref. [58] and subsequently reexamined in Ref. [59]. Indeed, the behavior of the charged-Higgs loop in the nondecoupling regime is similar to the contribution of a heavy fermion loop to the $h \to \gamma\gamma$ amplitude, which scales as $G_{h\bar{f}f}/m_f$ and approaches a constant for $m_f \gg m_h$. In particular, if m_f is too large, then $G_{h\bar{f}f} = m_f/v \gg 1$ and tree-level unitarity is violated. However, there is an intermediate range of heavy fermion masses above m_h but below the mass scale at which tree-level unitarity is violated, in which the fermion loop contribution to the $h \to \gamma\gamma$ amplitude is approximately constant. Likewise, if $G_{hH^+H^-}/v \gg 1$ is too large then one would need to take Z_3 above its unitarity bound [in light of Eq. (3.26)]. Again, there is an intermediate region of heavy Higgs masses (where tree-level unitarity is still maintained) in which the charged-Higgs loop contribution to the $h \to \gamma\gamma$ amplitude is approximately constant. Thus, we expect regions of 2HDM parameter space in which a SM-like Higgs can exhibit a nonnegligible deviation in $\Gamma(h \to \gamma\gamma)$ from SM expectations.

Alternatively, the second term on the right-hand side of Eq. (3.27) can be enhanced in the delayed decoupling regime where $\tan\beta \gg 1$ and $|\cos(\beta - \alpha)|\tan\beta \sim \mathcal{O}(1)$. In this case, $G_{hH^+H^-} \sim \mathcal{O}(m_A^2/v) \sim \mathcal{O}(m_{H^\pm}^2/v)$ [under the assumption that λ_4, $\lambda_5 \lesssim \mathcal{O}(1)$]. However, this behavior is also associated with growing quartic couplings that can potentially violate tree-level unitarity. Indeed, by comparing with Eq. (3.26), we see that Z_7 is being enhanced. More directly, it is straightforward to obtain

$$(m_A^2 - m_h^2 + \lambda_5 v^2)(\cot\beta - \tan\beta)\cos(\beta - \alpha)$$
$$= -v^2\cos 2\beta[(\lambda_1 - \lambda_3 - \lambda_4 - \lambda_5)\cos\beta\sin\alpha$$
$$+ (\lambda_2 - \lambda_3 - \lambda_4 - \lambda_5)\sin\beta\cos\alpha], \quad (3.29)$$

---

[8]The contribution of the $W^\pm$ loop deviates from the SM by a factor of $\mathcal{O}(\cos^2(\beta - \alpha))$ in light of Eq. (3.1).

which again implies that some of the Higgs potential parameters must be enhanced by a factor of $\mathcal{O}(m_A^2/v^2)$ if $m_A^2 \gg v^2$ and $|\cos(\beta - \alpha)| \tan\beta \sim \mathcal{O}(1)$. Thus, if m_A becomes too large, the unitarity constraints on the Higgs potential quartic coupling parameters will be violated. Nevertheless, there exists an intermediate range of charged-Higgs masses in which tree-level unitarity is maintained while the charged-Higgs loop contribution to the $h \to \gamma\gamma$ amplitude is approximately constant. That is, there exists a region of 2HDM parameter space, in which $|\cos(\beta - \alpha)|$ is small and the $h\bar{D}D$ coupling is opposite in sign to that of the SM Higgs boson, where a deviation in the $h \to \gamma\gamma$ decay rate from the predicted SM rate due to the contribution of the charged-Higgs loop can be detected.

Details on the nondecoupling of the $H^\pm$ loop contribution to the $h \to \gamma\gamma$ amplitude can be found in Appendix C, where it is shown that such nondecoupling is inevitable for the wrong-sign $h\bar{D}D$ coupling scenario. The resulting magnitude of the effect yields deviations from the SM that will ultimately be observable at the LHC and a future linear collider, as discussed in the following sections.

IV. PHENOMENOLOGY OF THE WRONG-SIGN YUKAWA COUPLINGS

It is convenient to define the ratio of the $h \to f$ coupling to the corresponding SM value as

$$\kappa_f = \frac{g_{hf}}{g_{h_{\mathrm{SM}}f}}, \tag{4.1}$$

where we will be considering $f = b\bar{b}$, $c\bar{c}$, $\tau^+\tau^-$, WW^*, ZZ^*. As for the coupling to photons, κ_γ is defined as

$$\kappa_\gamma^2 = \frac{\Gamma^{\mathrm{2HDM}}(h \to \gamma\gamma)}{\Gamma(h_{\mathrm{SM}} \to \gamma\gamma)}, \tag{4.2}$$

with an analogous definition for κ_g. Note that κ_γ and κ_g are strictly positive, whereas the remaining κ_f could be either positive or negative. These definitions for the couplings κ coincide with the definitions used by the experimental groups at the LHC [60], at leading order. We shall also make the simplifying assumption (which holds in the SM and in the 2HDM under consideration) that all down-type [up-type] fermion final states are governed by the same κ_D [κ_U]. It is convenient to begin with a simplified discussion of the impact of changing the sign of κ_D in order to set the stage. In this section, we employ the convention of $|\alpha| \leq \pi/2$ for which $\kappa_U > 0$ in both type-I and type-II models. For this choice, the hVV coupling of Eq. (2.4) can, in principle, be either positive or negative. However, for $\kappa_U > 0$, the phenomenology of the $\gamma\gamma$ final state requires that the hVV coupling be positive, which means that acceptable regions of parameter space must have $\beta - \alpha > 0$.

Consider first the amplitude of the process $h \to gg$. In an appropriate normalization, the top- and bottom-quark loops contribute 4.1289 and $-0.2513 + 0.3601i$, respectively,

when $\kappa_U = 1$ and $\kappa_D = 1$. This implies a large fractional change in the ggh coupling with a change of sign of κ_D. One finds a shift in κ_g of $+13\%$ in going from positive $\kappa_D = +1$ to $\kappa_D = -1$. Naively, one would suppose that this large shift would be easily observed. However, this is a difficult task at the LHC due to the challenge in identifying gluons (even if indirectly) in the final state. In addition, the primary gg fusion production cross section has some systematic errors associated with higher order corrections. Nonetheless, Table 1-20 of Ref. [61] gives expected errors for κ_g of 6–8% for $L = 300~\mathrm{fb}^{-1}$ and 3%–5% for $L = 3000~\mathrm{fb}^{-1}$, based on fitting all the rates rather than directly observing the gg final state. At the ILC, the primary production mechanism of $e^+e^- \to Z^* \to Zh$ is very well determined in terms of the ZZh coupling and isolation of the gg final state is easier. The error on κ_g estimated in Ref. [61] is 2% for a combination of $L = 250~\mathrm{fb}^{-1}$ at $\sqrt{s} = 250$ GeV and $L = 500~\mathrm{fb}^{-1}$ at $\sqrt{s} = 500$ GeV. Other error estimates are to be found in Ref. [51,62] where it is concluded that κ_g can be measured at the ILC with an accuracy of 8.5% at a center-of-mass (CM) energy of 250 GeV and 7.3% at a CM energy of 350 GeV with an integrated luminosity of 250 fb^{-1} and beam polarization of -80% (electron) and 30% (positron) [62]. The error estimate for 500 GeV with $L = 500~\mathrm{fb}^{-1}$ decreases to $\sim 2.3\%$ (see Tables 6.1 and 6.2 of Ref. [51]), consistent with the estimate from Ref. [61]. Thus, in the end, we can anticipate that both the LHC and ILC will be able to determine whether or not h_D is positive using the indirect fit and direct measurement of κ_g, respectively.

In $h \to \gamma\gamma$, the presence of the large W-boson loop contribution means that considerable precision is required to identify the interference effects. In more detail, the contributions to the amplitude of this process assuming SM couplings are as follows [these are the I^h's defined in Eq. (C5)]; W boson, -8.3233; top-quark loop (with $\kappa_U > 0$), 1.8351; bottom loop for $\kappa_D > 0$, $-0.0279 + 0.0400i$. As a result, switching the sign of κ_D would change κ_γ from 1 to 0.991, i.e. a $\lesssim 1\%$ shift. The accuracy with which κ_γ can be measured at the 14 TeV LHC is given in Table 1-20 of Ref. [61] as 5%–7% for integrated luminosity of $L = 300~\mathrm{fb}^{-1}$ and 2%–5% for $L = 3000~\mathrm{fb}^{-1}$. The ranges correspond to optimistic/pessimistic estimates regarding systematic and theoretical errors. Thus, if the change in κ_γ was only of order 1% this could not be detected at the LHC. Nonetheless, we claim that with high enough integrated luminosity one can distinguish $\kappa_D < 0$ from $\kappa_D > 0$ in the context of the type-II 2HDM using the high precision $\gamma\gamma$ final state due to the fact that the $\gamma\gamma h$ coupling is inevitably suppressed in the $\kappa_D = -1$ case as a result of a large nondecoupling charged-Higgs loop contribution, i.e. one that approaches a constant at large charged-Higgs mass (up to the limit at which the λ_i couplings violate the tree-level unitarity bounds). There is also a $\kappa_D > 0$ region of parameter space for which the charged-Higgs loop does not decouple, and this region would
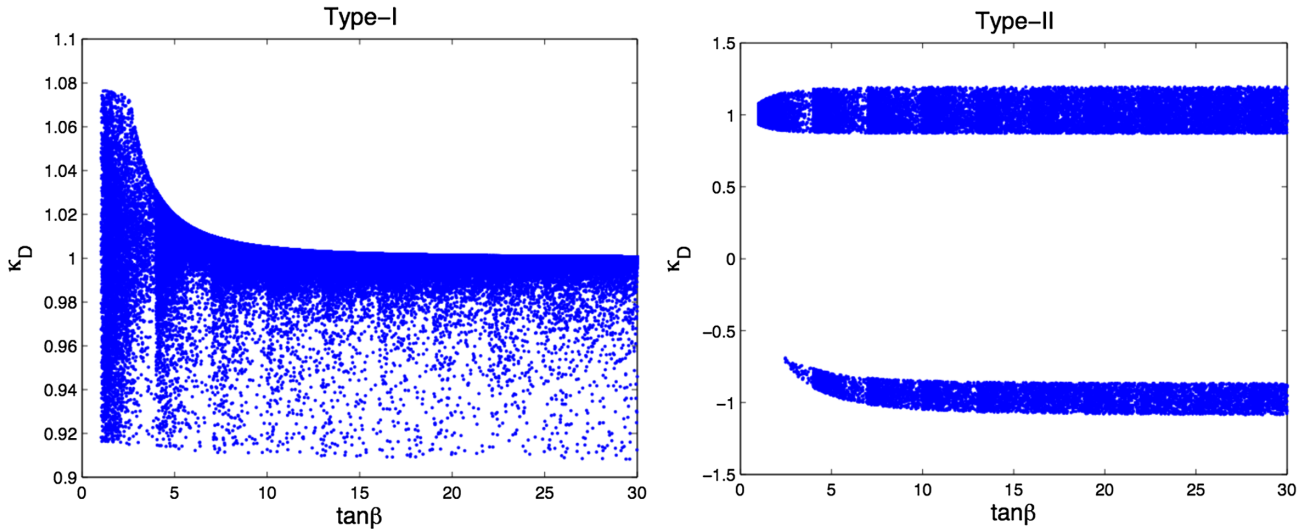
FIG. 1 (color online).   Ratio of the lightest Higgs couplings to down quarks in the 2HDM relative to the SM as a function of $\tan\beta$. Left: Type-I and right: type-II. All $\mu_f^h(\text{LHC})$ are within 20% of the SM value.

be ruled out in very similar fashion to the $\kappa_D < 0$ region we focus on. In fact, the modification to the $\gamma\gamma$ coupling is the *only* way of revealing this $\kappa_D > 0$ nondecoupling region. However, for $\kappa_D > 0$ there is also the standard decoupling region for which the charged-Higgs loop does decouple and that would allow arbitrarily precise agreement with the SM predictions. A detailed discussion of nondecoupling and perturbativity/unitarity bounds is given in Appendix C. Typically, κ_γ is inevitably suppressed relative to the SM prediction by about 5% for $\kappa_D < 0$, which should be measurable at the $\sqrt{s} = 14$ TeV LHC run for $L = 3000$ fb^{-1}. At the ILC, for a combination of $L = 250$ fb^{-1} at $\sqrt{s} = 250$ GeV and $L = 500$ fb^{-1} at $\sqrt{s} = 500$ GeV the expected error on κ_γ is $\sim 8.3\%$ (including a 0.5% theory uncertainty) based on measuring $e^+e^- \to Zh$ with $h \to \gamma\gamma$, implying that the sign of κ_D cannot be directly determined at the ILC using the $\gamma\gamma$ final state.

To explore in more detail, we scan over the 2HDM parameter space subject to all the constraints described in Sec. II. We begin by fixing $m_h = 125$ GeV. The charged-Higgs mass is varied between 100 and 900 GeV in type-I and 340 and 900 GeV in type-II. The heavier CP-even scalar mass was kept between 125 and 900 GeV while the pseudoscalar mass range is between 90 and 900 GeV. The soft-breaking parameter was varied in the range $-(900 \text{ GeV})^2 < m_{12}^2 < (900 \text{ GeV})^2$ while $1 < \tan\beta < 30$. After passing all constraints, the points were used to calculate the various $\mu_f^h(\text{LHC})$, which is the ratio of the number of events predicted by the model for the process $pp \to h \to f$ to the SM prediction for the same final state,

$$\mu_f^h(\text{LHC}) = \frac{\sigma^{2\text{HDM}}(pp \to h)\text{BR}^{2\text{HDM}}(h \to f)}{\sigma^{\text{SM}}(pp \to h_{\text{SM}})\text{BR}(h_{\text{SM}} \to f)}. \quad (4.3)$$

In computing the $pp \to h$ cross section, we have summed over all light Higgs production mechanisms (gg fusion, VV fusion, Vh associated production, $b\bar{b}$ fusion, and $t\bar{t}h$ associated production),[9] employing a mass of $m_h = 125$ GeV. The processes that involve only Higgs couplings to gauge bosons can be obtained by simply rescaling the SM cross sections. Hence, for Higgs Strahlung and vector boson fusion we have used the results of Ref. [63] (the same applies to the final state $ht\bar{t}$). We have included QCD corrections but not the SM electroweak corrections because they can be quite different for the 2HDMs. Cross sections for $b\bar{b} \to h$ are included at next-to-next-to-leading order (NNLO) [64] and the gluon fusion process $gg \to h$ was calculated using HIGLU [65]. (When the Higgs boson is SM-like, the $b\bar{b} \to h$ cross section is much smaller than the $gg \to h$ cross section.) Our baseline will be to require that the $\mu_f^h(\text{LHC})$ for final states $f = WW$, ZZ, $b\bar{b}$, $\gamma\gamma$ and $\tau^+\tau^-$ are each consistent with unity within 20%, which is a rough approximation to the precision of current data. We then examine the consequences of requiring that all the $\mu_f^h(\text{LHC})$ be within 10% or 5% of the SM prediction. This enables us to understand how an increase in precision affects the scenario we will now describe in detail.

As discussed in Secs. II and III, the relative hVV coupling is given by $\kappa_V = g_{hVV}^{2\text{HDM}}/g_{hVV}^{\text{SM}} = \sin(\beta - \alpha)$. The relative Higgs-fermion couplings are $\kappa_U = \kappa_D = \cos\alpha/\sin\beta$ in the type-I 2HDM, whereas in the type-II 2HDM,

---

[9]Further discrimination among models and parameter choices within a model can be obtained by separately considering each individual initial state × final state combination, as is now done by the LHC experimental collaborations and considered in Ref. [8].

$$\kappa_U = \frac{\cos\alpha}{\sin\beta}, \qquad \kappa_D = -\frac{\sin\alpha}{\cos\beta}. \qquad (4.4)$$

In Fig. 1 we show κ_D in type-I and type-II models as a function of $\tan\beta$ for those parameter space points that pass all theoretical and experimental constraints and have all $\mu_f^h(\text{LHC})$ within 20% of the SM prediction of 1. In all cases, $\kappa_V > 0$, which implies that a wrong-sign Yukawa coupling would correspond to a negative value of κ_D or κ_U. Noting that $\kappa_U \geq 0$ in the convention of $|\alpha| \leq \pi/2$, it follows that only regions with $\kappa_D < 0$ correspond to a wrong-sign Yukawa coupling scenario.

As expected, the left panel of Fig. 1 shows that all points are very close to $\kappa_D = 1$ for a type-I 2HDM, while the right panel shows that in the case of the type-II 2HDM all points fall within two main regions: one where $\kappa_D \approx 1$ and the other one where $\kappa_D \approx -1$. In short, although the LHC results have clearly shown that the Higgs rates to fermions and gauge bosons are very consistent with the SM predictions, it is clear that the roughly 20% precision with which LHC rates are currently measured allows for a second non-SM-like region with the opposite sign of h_D that can fit within the context of the type-II 2HDM.

In Sec. III, we showed that in the type-II 2HDM, the $\kappa_D \sim +1$ region corresponds to the limit $\sin(\beta-\alpha) \approx 1$ whereas the $\kappa_D \sim -1$ region is attained in the limit $\sin(\beta+\alpha) \approx 1$,

$$\kappa_D^{II} \to 1 \qquad (\sin(\beta-\alpha) \to 1);$$
$$\kappa_D^{II} \to -1 \qquad (\sin(\beta+\alpha) \to 1), \qquad (4.5)$$

corresponding to negative and positive values of $\sin\alpha$, respectively (in a convention where $0 \leq \beta \leq \frac{1}{2}\pi$). On the other hand, the relative hVV and hhh couplings satisfy

$$\kappa_V, \frac{G_{hhh}^{2HDM}}{G_{hhh}^{SM}} \to 1 \qquad (\sin(\beta-\alpha) \to 1);$$

$$\kappa_V, \frac{G_{hhh}^{2HDM}}{G_{hhh}^{SM}} \to \frac{\tan^2\beta - 1}{\tan^2\beta + 1}(\sin(\beta+\alpha) \to 1). \qquad (4.6)$$

In Fig. 2, the left panel shows $\tan\beta$ as a function of $\sin\alpha$ with all $\mu_f^h(\text{LHC})$ within 20% (blue/black), 10% (green/light grey) and 5% (red/dark grey) of their SM values. We clearly see two branches—one with $\sin\alpha < 0$ corresponding to the SM limit and one with $\sin\alpha > 0$ corresponding to the wrong-sign Yukawa coupling scenario. In the left branch, the points are all such that $\sin(\beta-\alpha) \sim 1$; the points in the right branch all have $\sin(\beta+\alpha) \sim 1$. The right panel shows that as $\tan\beta$ increases the $\kappa_D < 0$ branch corresponds to parameters with small $\cos(\beta-\alpha)$, i.e. $\sin(\beta-\alpha) \sim 1$. Note that the second branch is excluded if we demand that all the $\mu_f^h(\text{LHC})$ fall within 5% of unity.

It is instructive to consider why $\sin(\beta+\alpha) \approx 1$ with $\kappa_D \sim -1$ is still allowed by current data. Note that Eq. (3.11) implies that at very large $\tan\beta$ where $\beta \to \frac{1}{2}\pi$,

$$\sin(\beta+\alpha) - \sin(\beta-\alpha) = \frac{2(1-\epsilon)}{1+\tan^2\beta} \ll 1$$

$$(\text{for } \tan\ \beta \gg 1). \qquad (4.7)$$

In particular, when $\epsilon < 1$ we see that $\sin(\beta-\alpha)$ is always below $\sin(\beta+\alpha)$. Figure 2 reflects the behavior shown in Eq. (4.7) in that the larger $\tan\beta$ is, the closer the negative and positive $\sin\alpha$ regions are. Furthermore, as ϵ decreases the region where the low values of $\tan\beta$ are allowed decreases. Therefore, when $\tan\beta$ is very large we see that $|\cos(\beta-\alpha)| \ll 1$, and we recover the SM VV and hhh couplings. Furthermore, as discussed earlier there is limited sensitivity to the sign of the Yukawa couplings for
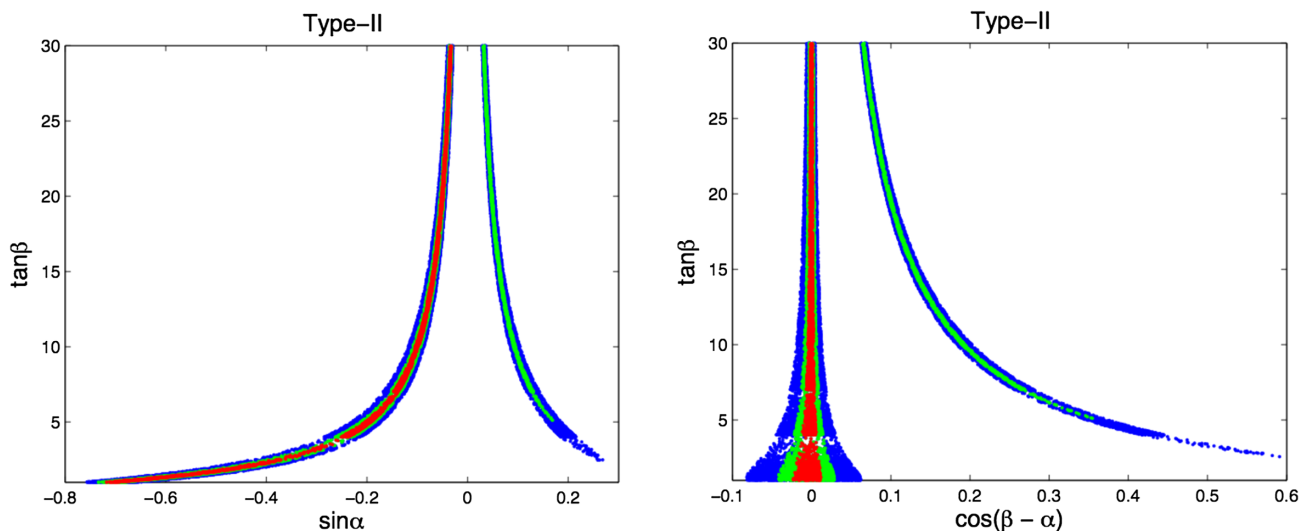

FIG. 2 (color online). Allowed regions for 2HDM type-II with all $\mu_f^h(\text{LHC})$ within 20% (blue/black), 10% (green/light grey) and 5% (red/dark grey) of the SM value of unity. Left: In the $\tan\beta$ vs $\sin\alpha$ plane. Right: In $\tan\beta$ vs $\cos(\beta-\alpha)$ space.
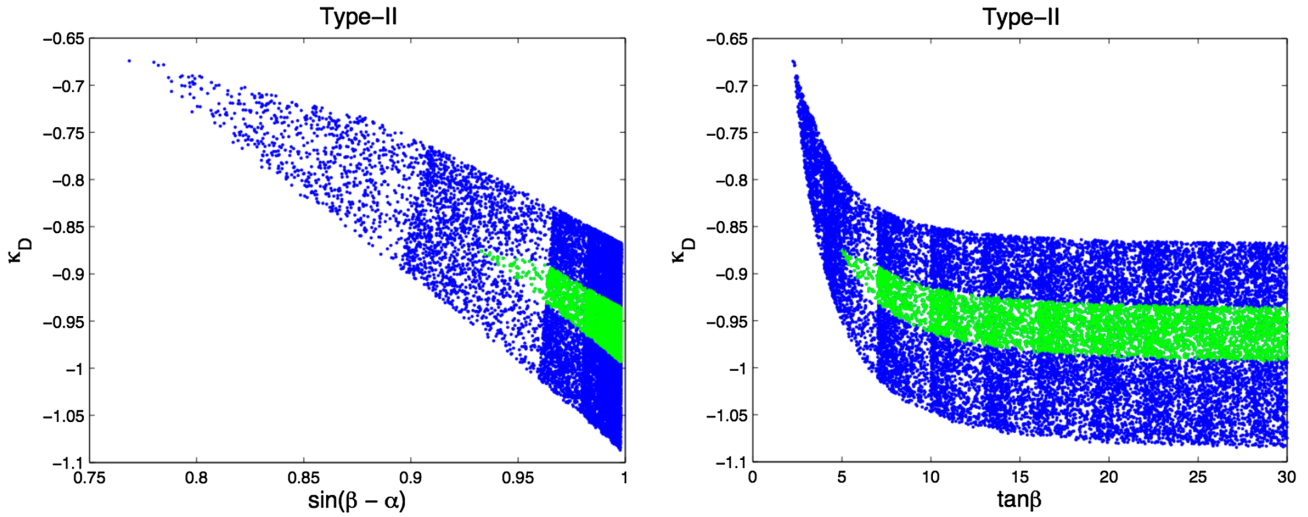
FIG. 3 (color online).   Left panel: The Yukawa coupling ratio $\kappa_D = h_D^{2HDM}/h_D^{SM}$ as a function of $\sin(\beta - \alpha)$ in the type-II 2HDM, with all μ_f^h(LHC) within 20% (blue/black) and 10% (green/light grey) of their SM values. Right panel: Same ratio as a function of $\tan\beta$. If one demands consistency at the 5% level, no points survive.

theone-loop induced $\gamma\gamma$ and gg couplings. Thus, due to the limited accuracy with which the $\gamma\gamma$ and gg couplings are (indirectly) measured, the region of wrong-sign Yukawa couplings [where $\sin(\beta + \alpha) \approx 1$ and $\sin\alpha > 0$] in the type-II 2HDM is still allowed by the current LHC data.

V. RESULTS AND DISCUSSION

In order to study in more detail the wrong-sign region of the type-II 2HDM, we have generated a new set of points where we have further imposed that $\sin\alpha > 0$. In the left panel of Fig. 3 we present κ_D as a function of $\sin(\beta - \alpha)$, with all μ_f^h(LHC) within 20% of the SM values in blue (black) and 10% of the SM values in green (light grey).
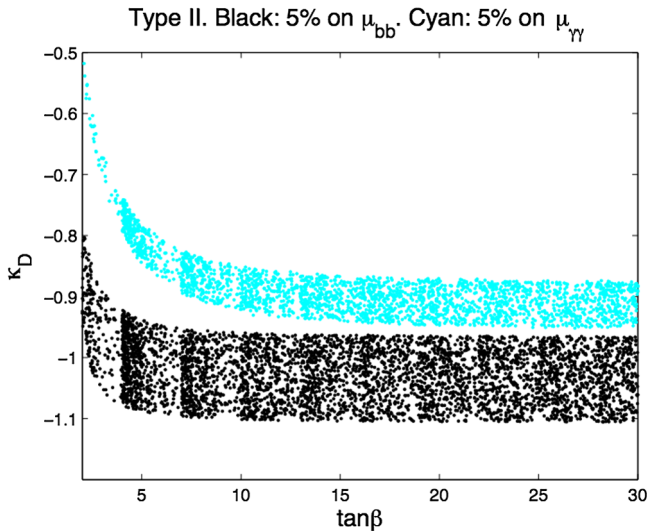
FIG. 4 (color online).   For the 2HDM type-II, we show regions in κ_D vs $\tan\beta$ space having $\sin\alpha > 0$ that are allowed when $\mu_{\gamma\gamma}^h$(LHC) (cyan/grey) and μ_{bb}^h(LHC) (black) are within 5% of the SM prediction of unity.

As expected, the values are very close to the region where $\kappa_D = -1$ while simultaneously $\sin(\beta - \alpha)$ approaches 1. As the μ_f^h(LHC) values are required to agree more precisely with the SM value of 1, the points move closer to the above limit. In the right panel we show the same ratio as a function of $\tan\beta$. As $\tan\beta$ grows, $\sin(\beta + \alpha)$ is forced to be closer to $\sin(\beta - \alpha)$ as indicated in Eq. (4.7) and is forced to be closer to 1 due to the LHC constraints. As indicated by Fig. 2, increasing the precision of the Higgs measurements would allow exclusion of the low $\tan\beta$ region if all μ_f^h(LHC) are within 10% of unity. Moreover, the entire $\kappa_D < 0$ region is eliminated if all μ_f^h(LHC) are within 5% of unity.

In fact, we will see that it is $\mu_{\gamma\gamma}^h$(LHC) that makes overall consistency with SM rates at the 5% level impossible in the $\sin\alpha > 0$ branch. This is due to the fact that for all the $\kappa_D < 0$ points we are in the nondecoupling regime for which the charged-Higgs boson loop contribution to the $h \to \gamma\gamma$ amplitude is approximately constant as a function of $m_{H^\pm}$ (up until the tree-level unitarity upper limit of $m_{H^\pm} \sim 650$ GeV, beyond which $\kappa_D < 0$ is not a perturbatively consistent possibility). The charged-Higgs loop gives about a 10% reduction in $\Gamma(h \to \gamma\gamma)$ that is inconsistent with $\mu_{\gamma\gamma}^h$(LHC) being within 5% of unity. The details of the nondecoupling regime are discussed at length in Appendix C.

Another perspective is obtained by examining Fig. 4. There, we have shown regions in κ_D vs $\tan\beta$ space where either $\mu_{\gamma\gamma}^h$(LHC) (cyan/grey) or μ_{bb}^h(LHC) (black) are within 5% of unity for points in the $\sin\alpha > 0$ branch.[10] We observe that the two branches represented do not intersect, and as such it is impossible to achieve 5% agreement with the SM in

---

[10]Note that $\mu_{\tau^+\tau^-}^h$(LHC) $= \mu_{bb}^h$(LHC) in the 2HDM, implying that measurements in the $\tau^+\tau^-$ channel are equally useful. Further, at the LHC, the $\tau^+\tau^-$ final state will be more precisely measured than for the $b\bar{b}$ final state.
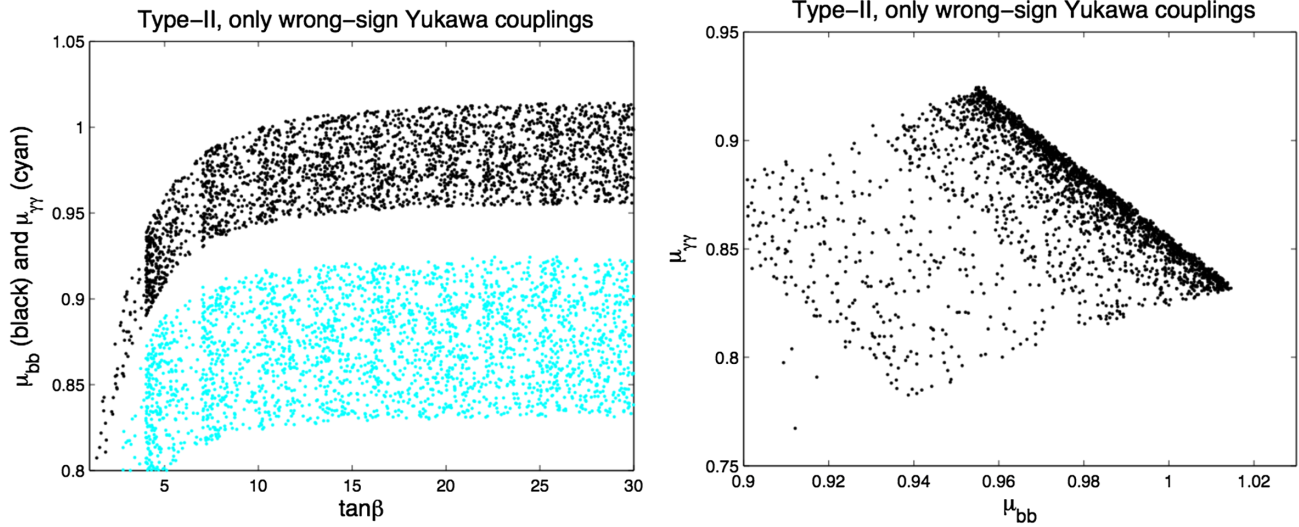
FIG. 5 (color online).   Assuming that the WW, ZZ rates are measured to be within 5% of the SM prediction, we plot $\mu_{\gamma\gamma}^h$(LHC) and μ_{bb}^h(LHC) vs $\tan\beta$ (left) and $\mu_{\gamma\gamma}^h$(LHC) vs μ_{bb}^h(LHC) (right).

both of these channels. This explains why there are no red points in the right branch of the plots in Fig. 2.

Further insight is gained from Fig. 5, which considers points for which the $\mu_{WW,ZZ}^h$(LHC) are within 5% of the SM value of 1. On the left, we exhibit the values of $\mu_{\gamma\gamma}^h$(LHC) and μ_{bb}^h(LHC) vs $\tan\beta$. This shows that while μ_{bb}^h(LHC) can be within 5% of unity, $\mu_{\gamma\gamma}^h$(LHC) cannot—it is always more than 7%–8% below unity, implying that 5% accuracy on this channel would exclude the $\kappa_D < 0$ branch. On the right, we plot $\mu_{\gamma\gamma}^h$(LHC) vs μ_{bb}^h(LHC). The largest value of $\mu_{\gamma\gamma}^h$(LHC) that can be achieved is ∼0.925, and this only if μ_{bb}^h(LHC) $\lesssim 0.96$. Thus, it is the suppression of the $\gamma\gamma$ final state at the LHC that is key to ruling out the $\kappa_D < 0$ possibility for $\sqrt{s} = 14$ TeV operation at high luminosity. This same conclusion is found in the work of Ref. [66]. There, different

initial states are separated from one another and one finds that the $VV \to h \to \gamma\gamma$ rate is the most suppressed relative to other processes—because of the 6% enhancement of $\sigma(gg \to h)$ when $\kappa_D < 0$ the $gg \to h \to \gamma\gamma$ rate is not as suppressed relative to the remaining processes but still contributes to the overall inconsistency for $\kappa_D < 0$ between these $\gamma\gamma$ final state channels with other final states such as ZZ, WW and $\tau\tau$ when all are measured with 5% accuracy.

In Fig. 6, we show in κ_γ or κ_g vs κ_D space the points that are allowed if the μ_f^h(LHC)'s are each within 20% (blue), 10% (green), or 5% (red) of unity (the SM limit). We observe from the left-hand plot that κ_γ is always at least 5% below unity in the $\kappa_D < 0$ region and that 5% accuracy on the μ_f^h(LHC)'s will eliminate this region entirely. In fact, as we saw in Fig. 5 it is $\mu_{\gamma\gamma}^h$(LHC) that necessarily has a greater than 5% deviation from unity. The right-hand plot
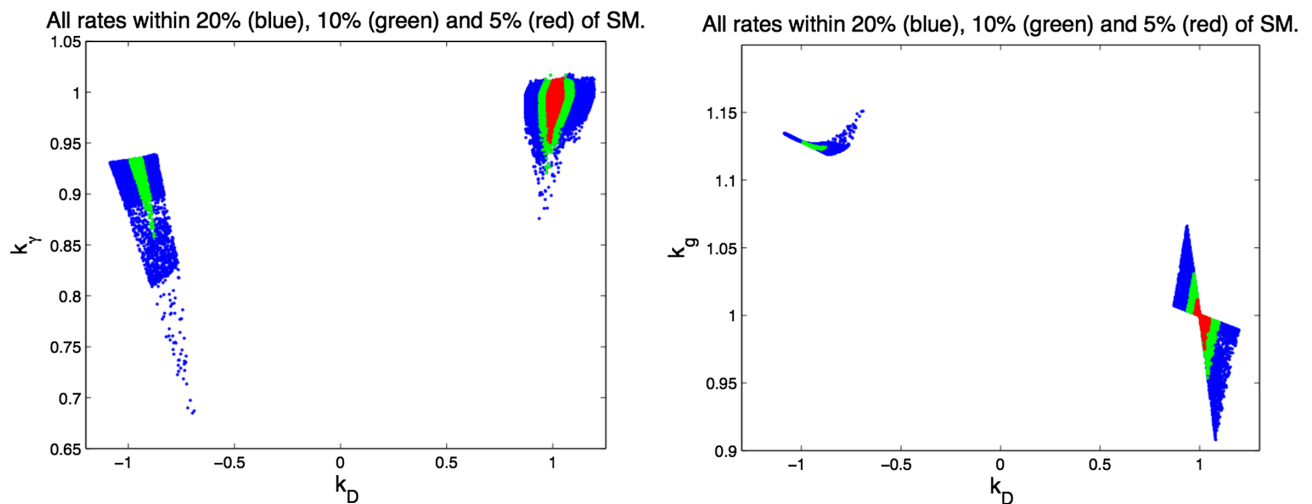

FIG. 6 (color online).   Allowed regions for 2HDM type-II with all μ_f^h(LHC) within 20% (blue/black), 10% (green/light grey) and 5% (red/dark grey) of their SM values in κ_γ vs κ_D space (left); κ_g vs κ_D space (right).
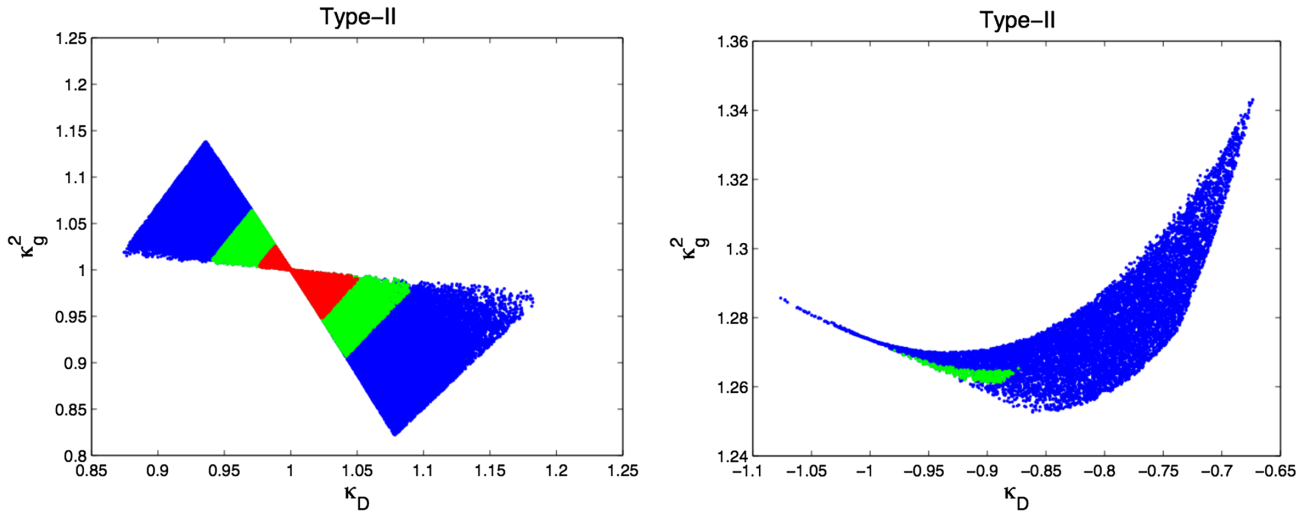
FIG. 7 (color online). $\kappa_g^2 = \Gamma(h \to gg)^{2\text{HDM}}/\Gamma(h_{\text{SM}} \to gg)$ as a function of $\kappa_D = h_D^{2\text{HDM}}/h_D^{\text{SM}}$ in type-II, with all $\mu_f^h(\text{LHC})$ within 20% (blue/black), 10% (green/light grey) and 5% (red/dark grey) of their SM values. Left panel: $\sin\alpha < 0$. Right panel: $\sin\alpha > 0$.

shows that in the $\kappa_D < 0$ region, κ_g is always bigger than 1.13. However, since currently the LHC is unable to determine κ_g with the necessary accuracy this does not help to exclude the $\kappa_D < 0$ region. But, as summarized earlier, with $L = 300$ fb^{-1} at $\sqrt{s} = 14$ TeV, κ_g can be determined to about 8% accuracy and such a deviation will certainly be observable.

As noted earlier, at the ILC the gg final state becomes a powerful tool for determining the sign of κ_D. Thus, we shall explore the gg final state issues in more detail. In Fig. 7 we exhibit $\kappa_g^2 = \Gamma(h \to gg)^{2\text{HDM}}/\Gamma(h_{\text{SM}} \to gg)$ as a function of κ_D for $\sin\alpha < 0$ (left) and $\sin\alpha > 0$ (right) with all $\mu_f^h(\text{LHC})$ within 20% of the SM values in blue (dark grey) and 10% of the SM values in green (light grey). Contrary to the SM-like scenario, when $\sin\alpha > 0$ (wrong-sign Yukawa coupling) the value of the ratio of the widths is always above 1.25. Figure 7 shows that the minimum value of κ_g^2 becomes larger when smaller deviations of the $\mu_f^h(\text{LHC})$s from unity are required. In particular, when the h_D coupling changes sign but all tree-level couplings have SM magnitude, the ratio between the two widths is exactly

$$\frac{\Gamma(h \to gg)^{2\text{HDM}}}{\Gamma(h_{\text{SM}} \to gg)} = 1.27 \quad (\sin(\beta + \alpha) = 1), \qquad (5.1)$$

which is in agreement with HDECAY [67,68] and 2HDMC [68,69]. Note that this interference effect, which is almost 30% relative to the SM, does not manifest itself in the production process $gg \to h$ that is important for the LHC and might therefore have been quite easily detectable. In contrast to the leading order (LO) result,

$$\frac{\sigma(gg \to h)_{\text{LO}}^{2\text{HDM}}}{\sigma(gg \to h_{\text{SM}})_{\text{LO}}} \approx \frac{\Gamma(h \to gg)_{\text{LO}}^{2\text{HDM}}}{\Gamma(h_{\text{SM}} \to gg)_{\text{LO}}} \approx 1.27$$
$$(\sin(\beta + \alpha) = 1), \qquad (5.2)$$

at NNLO in the limit of $\sin(\beta + \alpha) = 1$, $\sigma(gg \to h)_{\text{NNLO}}^{2\text{HDM}}/\sigma(gg \to h_{\text{SM}})_{\text{NNLO}} \approx 1.06$ [65] while the ratio of the partial widths of $h \to gg$ does not suffer any significant change in going from LO to NNLO. Therefore, the present LHC data cannot discriminate between the two scenarios based on interference effects at the production level; it is only through a luminosity $L \geq 300$ fb^{-1} of data accumulated at $\sqrt{s} = 14$ TeV and a combined fit of the rates for all final states that one can manage to determine the underlying κ_g with adequate precision.

Of course the ILC can probe BR$(h \to gg)$ more easily and directly using the process $e^+ e^- \to Zh \to Zgg$. We define

$$\mu_{gg}^h(\text{ILC}) = \frac{\sigma \text{BR}(h \to gg)}{\sigma^{\text{SM}} \text{BR}(h_{\text{SM}} \to gg)} \qquad (5.3)$$

where σ is the measured $e^+ e^- \to Z^* \to Zh$ Higgs production cross section at the ILC and σ^{SM} and BR$(h_{\text{SM}} \to gg)$ are the SM values of the production cross section at the ILC and branching ratio of a Higgs decaying to a pair of gluons. The ratio of the cross sections in the process $e^+ e^- \to Zh$ is just $\sin^2(\beta - \alpha)$. Likewise we can define similar ratios for the processes $e^+ e^- \to Zh \to Zb\bar{b}$ and $e^+ e^- \to Zh \to Zc\bar{c}$ which we will call $\mu_{bb}^h(\text{ILC})$ and $\mu_{cc}^h(\text{ILC})$, respectively.

In the left panel of Fig. 8 we show the quantity $\mu_{gg}^h(\text{ILC})$ as a function of $\tan\beta$. When all $\mu_f^h(\text{LHC})$'s measured at the LHC are forced to be within 20% of the SM values (blue/black) all points are above 1.12. If the precision is increased to 10%, the bound is increased to 1.25. Recently, it was shown that $\mu_{gg}^h(\text{ILC})$ can be measured at the ILC with an accuracy of 8.5% at a CM energy of 250 GeV and 7.3% at a CM energy of 350 GeV with an integrated luminosity of 250 fb^{-1} and beam polarization of -80% (electron) and 30% (positron) [51,62]. The 95% C.L. predicted measurement for $\sqrt{s} = 350$ GeV and 250 fb^{-1} luminosity is
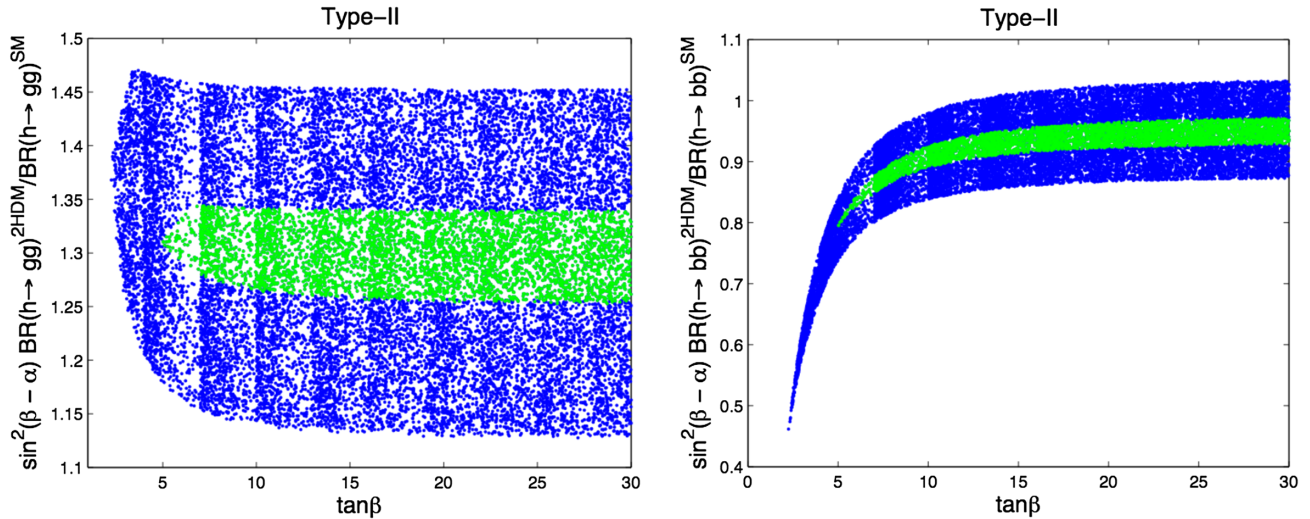
FIG. 8 (color online).   Left panel: μ_{gg}^h(ILC) as a function $\tan\beta$. Right panel: μ_{bb}^h(ILC) as a function of $\tan\beta$. The model is type-II, requiring $\sin\alpha > 0$, with all μ_f^h(LHC) within 20% of the SM values in blue (black) and 10% of the SM values in green (light grey).

1.02 ± 0.07 [62], assuming SM expectations. Therefore, this measurement could exclude all points in the left panel of Fig. 8. In the right panel we present μ_{bb}^h(ILC) as a function of $\tan\beta$. The corresponding SM predicted measurement for the ILC is 1.00 ± 0.01. Clearly, a better than about 5% measurement of μ_{bb}^h(ILC) can also help probe the wrong-sign coupling provided enough precision is attained at the LHC in the measurements of the Higgs couplings to fermions and gauge bosons. The values of μ_{bb}^h(ILC) are slightly below 1 because, as can be seen from Eq. (4.7), when $\sin(\beta + \alpha) \to 1$, $\sin(\beta - \alpha)$ is slightly below 1 as the right-hand side of the equation is positive. Note that the ratio of the branching ratios in μ_{bb}^h(ILC) is very close to 1 in the limit we are considering and as such μ_{bb}^h(ILC) $\approx \sin^2(\beta - \alpha)$. Similar results would be obtained for μ_{cc}^h(ILC), where the final state is $c\bar{c}$, but the precision in the μ_{cc}^h(ILC) measurement is not as good as for μ_{bb}^h(ILC).

VI. CONCLUSIONS

The couplings of the Higgs boson recently discovered at the LHC to the fermions and gauge bosons are starting to be measured with some precision. It is important to understand the implications of these results in the context of specific Higgs sector models. In this paper, we considered type-I and type-II $\mathbb{Z}_2$-symmetric and *CP*-conserving 2HDMs. Our focus was on the fact that the sign of the Yukawa coupling to the down-type fermions could be opposite to that of the SM. Using scans over type-I and type-II parameter spaces, subject to basic theoretical and experimental constraints as described in the main text, we found that a sign change in the down-quark Yukawa couplings can be accommodated in the context of the current LHC data set at 95% C.L., but only in the case of the type-II 2HDM

when $\sin(\beta + \alpha) \sim 1$. The situation is different in the type-I 2HDM—because only one doublet couples to all fermions the sign change would result in deviations from the SM predictions that are incompatible with the current Higgs data set. In this paper, we address the possibility of probing the wrong-sign Yukawa coupling of the Higgs to down-type quarks with future measurements of Higgs properties at the $\sqrt{s} = 14$ TeV LHC and at the International Linear Collider.

In particular, we performed a scan dedicated to the part of type-II 2HDM parameter space where the wrong-sign down-type quark coupling is currently acceptable. We filtered parameter space points requiring that the values of μ_f^h(LHC), the production rate of a given final state f relative to the SM, are within either 20%, 10% or 5% of the SM predictions for the LHC. Of greatest immediate interest is the fact that projected precisions for the determination of the magnitude of the $\gamma\gamma h$ coupling relative to its SM value, κ_γ (using $pp \to h \to \gamma\gamma$ in particular) imply that the LHC with $\sqrt{s} = 14$ TeV and $L \geq 300$ fb^{-1} will either rule out or confirm the wrong-sign scenario. Of particular importance for this conclusion is the fact that the charged-Higgs loop contribution to the $\gamma\gamma h$ couplings does not decouple for the $\sin(\beta + \alpha) \to 1$ scenario, leading to a $\sim 10\%$ decrease in $\Gamma(h \to \gamma\gamma)$. This statement applies for any charged-Higgs mass below the bound of about 650 GeV for which the Higgs coupling parameters satisfy tree-level unitarity bounds. In the context of the model, a finding that the h_D Yukawa has a negative sign *and also* detecting a charged-Higgs with mass above 650 GeV would imply that the theory is in a realm where perturbative calculations become suspect.

In addition, we have shown that the predictions for the measurements of μ_{gg}^h(ILC) and μ_{bb}^h(ILC) at the ILC would

allow us to probe the wrong-sign Yukawa coupling of a type-II 2HDM. Therefore, at both collider facilities, either a measurement or a definite 95% exclusion limit could be set on the wrong-sign Yukawa coupling scenario.

APPENDIX A: THE HIGGS BASIS OF THE SOFTLY BROKEN $\mathbb{Z}_2$-SYMMETRIC *CP*-CONSERVING 2HDM

It is convenient to reexpress the Higgs potential given by Eq. (2.2) in the Higgs basis [41–47]. By assumption, we have assumed that all the scalar potential parameters and the two vacuum expectation values v_1 and v_2 are real, which implies that the scalar potential and the vacuum are *CP* invariant. By a suitable transformation on the two-Higgs-doublet fields Φ_a ($a = 1, 2$), one can define two new linearly independent Higgs doublet fields H_1 and H_2 such that $\langle H_1^0 \rangle = v/\sqrt{2}$ and $\langle H_2^0 \rangle = 0$. This is accomplished by defining

$$H_1 = \begin{pmatrix} H_1^+ \\ H_1^0 \end{pmatrix} \equiv \frac{v_1 \Phi_1 + v_2 \Phi_2}{v},$$

$$H_2 = \begin{pmatrix} H_2^+ \\ H_2^0 \end{pmatrix} \equiv \frac{-v_2 \Phi_1 + v_1 \Phi_2}{v}. \tag{A1}$$

The Higgs basis is uniquely defined up to an overall sign of the H_2 scalar doublet field. In the Higgs basis, the scalar potential is given by

$$\mathcal{V} = Y_1 H_1^\dagger H_1 + Y_2 H_2^\dagger H_2 + [Y_3 H_1^\dagger H_2 + \text{H.c.}] + \frac{1}{2} Z_1 (H_1^\dagger H_1)^2 + \frac{1}{2} Z_2 (H_2^\dagger H_2)^2 + Z_3 (H_1^\dagger H_1)(H_2^\dagger H_2)$$
$$+ Z_4 (H_1^\dagger H_2)(H_2^\dagger H_1) + \left\{ \frac{1}{2} Z_5 (H_1^\dagger H_2)^2 + [Z_6 (H_1^\dagger H_1) + Z_7 (H_2^\dagger H_2)] H_1^\dagger H_2 + \text{H.c.} \right\}, \tag{A2}$$

where the squared-mass terms are given by

$$Y_1 = m_{11}^2 \cos^2\beta + m_{22}^2 \sin^2\beta - 2 m_{12}^2 \sin\beta\cos\beta, \tag{A3}$$

$$Y_2 = m_{11}^2 \sin^2\beta + m_{22}^2 \cos^2\beta + 2 m_{12}^2 \sin\beta\cos\beta, \tag{A4}$$

$$Y_3 = (m_{22}^2 - m_{11}^2) \sin\beta\cos\beta - m_{12}^2 \cos 2\beta, \tag{A5}$$

and the Higgs basis quartic couplings are given by

$$Z_1 \equiv \lambda_1 \cos^4\beta + \lambda_2 \sin^4\beta + 2(\lambda_3 + \lambda_4 + \lambda_5) \sin^2\beta\cos^2\beta, \tag{A6}$$

$$Z_2 \equiv \lambda_1 \sin^4\beta + \lambda_2 \cos^4\beta + 2(\lambda_3 + \lambda_4 + \lambda_5) \sin^2\beta\cos^2\beta, \tag{A7}$$

$$Z_i \equiv (\lambda_1 + \lambda_2 - 2\lambda_3 - 2\lambda_4 - 2\lambda_5) \sin^2\beta\cos^2\beta + \lambda_i,$$
$$\text{for } i = 3, 4, 5, \tag{A8}$$

$$Z_6 \equiv -\sin\beta\cos\beta[\lambda_1 \cos^2\beta - \lambda_2 \sin^2\beta - (\lambda_3 + \lambda_4 + \lambda_5) \cos 2\beta], \tag{A9}$$

$$Z_7 \equiv -\sin\beta\cos\beta[\lambda_1 \sin^2\beta - \lambda_2 \cos^2\beta + (\lambda_3 + \lambda_4 + \lambda_5) \cos 2\beta]. \tag{A10}$$

Note that one is free to redefine Y_3, Z_6 and Z_7 by an overall sign in light of the sign ambiguity in defining the Higgs basis. The potential minimum conditions are especially simple in the Higgs basis,

$$Y_1 = -\frac{1}{2} Z_1 v^2, \qquad Y_3 = -\frac{1}{2} Z_6 v^2, \tag{A11}$$

leaving Y_2 as the only free squared-mass parameter of the model.

Finally, we note some useful relations that relate the Higgs basis parameters to the Higgs masses [16,70]:

$$Z_1 v^2 = m_h^2 \sin^2(\beta - \alpha) + m_H^2 \cos^2(\beta - \alpha), \tag{A12}$$

$$Z_3 v^2 = 2(m_{H^\pm}^2 - Y_2), \tag{A13}$$

$$Z_4 v^2 = m_h^2 \cos^2(\beta - \alpha) + m_H^2 \sin^2(\beta - \alpha) + m_A^2 - 2 m_{H^\pm}^2, \tag{A14}$$

$$Z_5 v^2 = m_h^2 \cos^2(\beta - \alpha) + m_H^2 \sin^2(\beta - \alpha) - m_A^2, \quad \text{(A15)}$$

$$Z_6 v^2 = -(m_H^2 - m_h^2) \sin(\beta - \alpha) \cos(\beta - \alpha). \quad \text{(A16)}$$

The Higgs masses and $\cos(\beta - \alpha)$ do not depend on the parameters Z_2 and Z_7.

APPENDIX B: THE WRONG-SIGN $h\bar{D}D$ COUPLING AND THE MSSM HIGGS SECTOR

The tree-level scalar potential of the MSSM Higgs sector is given by Eq. (2.2), with [11]

$$\lambda_1 = \lambda_2 = \frac{1}{4}(g^2 + g'^2), \qquad \lambda_3 = \frac{1}{4}(g^2 - g'^2),$$

$$\lambda_4 = -\frac{1}{2}g^2, \qquad \lambda_5 = 0. \quad \text{(B1)}$$

In particular $\lambda_6 = \lambda_7 = 0$ [defined below Eq. (2.2)]. Inserting Eq. (B1) into Eqs. (A6)–(A10) yields [70]

$$Z_1 = Z_2 = \frac{1}{4}(g^2 + g'^2)\cos^2 2\beta, \qquad Z_3 = Z_5 + \frac{1}{4}(g^2 - g'^2),$$

$$Z_4 = Z_5 - \frac{1}{2}g^2, \qquad Z_5 = \frac{1}{4}(g^2 + g'^2)\sin^2 2\beta,$$

$$Z_7 = -Z_6 = \frac{1}{4}(g^2 + g'^2)\sin 2\beta \cos 2\beta. \quad \text{(B2)}$$

Using the result for Z_6 given above in Eqs. (3.2) and (3.3) yields the tree-level expressions,

$$\cos^2(\beta - \alpha) = \frac{m_Z^2 \cos^2 2\beta - m_h^2}{m_H^2 - m_h^2}, \quad \text{(B3)}$$

$$\sin(\beta - \alpha)\cos(\beta - \alpha) = \frac{m_Z^2 \sin 2\beta \cos 2\beta}{m_H^2 - m_h^2}, \quad \text{(B4)}$$

where $m_{h,H}^2$ are the MSSM *tree-level CP*-even Higgs squared masses,

$$m_{H,h}^2 = \frac{1}{2}\left(m_A^2 + m_Z^2 \pm \sqrt{(m_A^2 + m_Z^2)^2 - 4m_Z^2 m_A^2 \cos^2 2\beta}\right). \quad \text{(B5)}$$

In addition, the MSSM tree-level Higgs-fermion Yukawa couplings possess a type-II structure due to supersymmetry.

In the decoupling limit where $m_H \sim m_A \gg m_Z$, Eq. (B3) implies that $\sin(\beta - \alpha) \simeq 1$ (in the convention where $0 \le \beta - \alpha \le \pi$). Using Eq. (B4),

$$\cos(\beta - \alpha)\tan\beta \simeq \frac{2m_Z^2 \sin^2\beta \cos 2\beta}{m_A^2} \ll 1, \quad \text{(B6)}$$

for *all* values of $\tan\beta$. In particular, for $\tan\beta \gg 1$, one can never have $\cos(\beta - \alpha)\tan\beta \sim \mathcal{O}(1)$ in the decoupling

regime. Thus, in the tree-level Higgs sector of the MSSM, the phenomenon of delayed decoupling discussed below Eq. (3.7) does not occur. In light of Eq. (3.4), one cannot achieve the wrong-sign $h\bar{D}D$ Yukawa coupling in the region of the tree-level MSSM Higgs sector parameter space where the hVV coupling is SM-like.

It is well known that radiative corrections can significantly alter the properties of the MSSM Higgs sector (reviewed in, e.g., Refs. [71] and [72]). In particular, the MSSM prediction for m_h^2 is significantly shifted from its tree-level value given in Eq. (B5) by radiative corrections [73]. In addition, the radiative corrections can also generate significant shifts to the tree-level values of the Higgs couplings. For example, consider the scenario in which the MSSM μ parameter and all supersymmetry-breaking mass parameters (excluding the B parameter, which fixes the value of the mass m_A) are all of order of a common supersymmetry-breaking mass scale M_{SUSY}. If $m_A \ll M_{\text{SUSY}}$, then one can integrate out all the supersymmetric states to obtain a low-energy effective theory below the scale M_{SUSY}, which can be identified as a 2HDM extension of the Standard Model. In this effective 2HDM, the tree-level values of the λ_i given in Eq. (B1) receive significant radiative corrections. Moreover, nonzero values for λ_5, λ_6 and λ_7 are generated [74], which can be complex if there are *CP*-violating phases associated with μ, A_t and the gluino mass parameter. Likewise, nonzero values for the so-called *wrong-Higgs* Yukawa couplings [75] that are absent in a type-II model are also generated. That is, the resulting effective 2HDM is no longer described by a softly broken $\mathbb{Z}_2$ symmetric 2HDM with type-II Higgs-fermion Yukawa couplings. Thus, the results of this paper are not directly applicable to the radiatively corrected MSSM Higgs sector with $m_A \ll M_{\text{SUSY}}$. Nevertheless, using the approximations given in Ref. [49], one can check whether it is possible to achieve a wrong-sign $h\bar{D}D$ coupling in a suitable region of the MSSM Higgs parameter space in which the radiative corrections to the Higgs couplings are potentially significant.

There are two separate effects that must be taken into account. First, the wrong-Higgs Yukawa couplings that are radiatively generated contribute an additional term to the $h\bar{D}D$ coupling, which is enhanced in the limit of large $\tan\beta$. Keeping only these $\tan\beta$-enhanced corrections, and neglecting any *CP*-violating phases of the MSSM parameters for simplicity, the following approximate expression (for $M_{\text{SUSY}} \gg m_Z$ and $\tan\beta \gg 1$) is given in Ref. [49] for the $hb\bar{b}$ coupling[11]:

$$g_{hb\bar{b}} = -\frac{m_b}{v}\frac{\sin\alpha}{\cos\beta}\left[1 - \frac{\Delta_b}{1 + \Delta_b}(1 + \cot\alpha\cot\beta)\right], \quad \text{(B7)}$$

where [77]

---

[11]The factor $(1 + \Delta_b)^{-1}$ in Eq. (B7) provides a resummation of the leading Δ_b corrections to all orders [76].

$$\Delta_b \simeq \left[\frac{2\alpha_s}{3\pi}\mu M_{\tilde{g}} I(M_{\tilde{b}_1}, M_{\tilde{b}_2}, M_{\tilde{g}})\right.$$
$$\left. + \frac{h_t^2}{16\pi^2}\mu A_t I(M_{\tilde{t}_1}, M_{\tilde{t}_2}, \mu)\right]\tan\beta. \qquad \text{(B8)}$$

In Eq. (B8), $M_{\tilde{g}}$ is the gluino mass, $M_{\tilde{b}_{1,2}}$ are the bottom squark masses, h_t is the top-quark Yukawa coupling and the loop integral $I(a, b, c)$ is given by

$$I(a, b, c)$$
$$= \frac{a^2 b^2 \ln(a^2/b^2) + b^2 c^2 \ln(b^2/c^2) + c^2 a^2 \ln(c^2/a^2)}{(a^2 - b^2)(b^2 - c^2)(a^2 - c^2)}.$$
$$\text{(B9)}$$

Note that $I(a, a, a) = 1/(2a^2)$. Thus, if all supersymmetric parameters appearing in Eq. (B8) are of $\mathcal{O}(M_{\text{SUSY}})$, then Δ_b approaches a constant (nondecoupling) value in the limit of $M_{\text{SUSY}} \gg m_Z$. It is convenient to rewrite

$$1 + \cot\alpha\cot\beta = \frac{\cos(\beta - \alpha)}{\sin\beta\sin\alpha}. \qquad \text{(B10)}$$

Inserting this result into Eq. (B7) and making use of Eq. (3.4), we end up with

$$g_{hb\bar{b}} = \frac{m_b}{v}\left[\sin(\beta - \alpha) - \cos(\beta - \alpha)\tan\beta\left(\frac{1 - \Delta_b\cot^2\beta}{1 + \Delta_b}\right)\right].$$
$$\text{(B11)}$$

Second, after integrating out the supersymmetric particles to obtain the low-energy effective 2HDM, one must take into consideration the renormalization of the CP-even mixing angle α. To include these effects, we diagonalize the radiatively corrected 2×2 CP-even Higgs squared-mass matrix. Denoting these loop corrections by $\delta\mathcal{M}_{ij}^2$, an approximate expression for $\cos(\beta - \alpha)$ in the limit of $m_Z \ll m_A \ll M_{\text{SUSY}}$ is given by [49]

$$\cos(\beta - \alpha)$$
$$\simeq \left(1 + \frac{\delta\mathcal{M}_{11}^2 - \delta\mathcal{M}_{22}^2}{2m_Z^2\cos 2\beta} - \frac{\delta\mathcal{M}_{12}^2}{m_Z^2\sin 2\beta}\right)\frac{m_Z^2\sin 2\beta\cos 2\beta}{m_A^2}.$$
$$\text{(B12)}$$

In the limit of $\tan\beta \gg 1$, the term proportional to $\delta\mathcal{M}_{12}^2$ in Eq. (B12) can dominate over the tree-level contribution. Using the approximate one-loop expression given in Ref. [49],

$$\cos(\beta - \alpha) \sim \frac{\delta\mathcal{M}_{12}^2}{m_A^2}$$
$$\simeq -\frac{g^2 m_t^4}{32\pi^2 m_W^2 m_A^2 \sin^2\beta}\frac{\mu X_t}{M_{\text{SUSY}}^2}\left(6 - \frac{X_t A_t}{M_{\text{SUSY}}^2}\right),$$
$$\text{(B13)}$$

where $X_t \equiv A_t - \mu\cot\beta$ (note that $X_t \simeq A_t$ for $\tan\beta \gg 1$).

A quick back-of-the-envelope numerical analysis can reveal whether it is possible to achieve a value of $vg_{hb\bar{b}}/m_b$ close to -1. We shall assume that $\sin(\beta - \alpha) \sim 1$, corresponding to a SM-like hVV coupling. To maximize the effect of the radiative corrections, we shall also assume that $\tan\beta \gg 1$. If we further assume that all supersymmetric particle masses are of $\mathcal{O}(M_{\text{SUSY}})$, then Eq. (B8) yields $\Delta_b \sim \pm 0.01\tan\beta$, where the sign is determined by the overall sign of $\mu M_{\tilde{g}}$ [since the first term in Eq. (B8) typically dominates]. In light of Eq. (3.6), we conclude that $|\Delta_b| \lesssim 0.5$, so at best the inclusion of Δ_b enhances the second term on the right-hand side of Eq. (B11) by a factor of 2. Thus, we examine whether it is plausible that $\cos(\beta - \alpha)\tan\beta \sim \mathcal{O}(1)$.

In evaluating Eq. (B13), we must also ensure that the observed Higgs mass is correctly reproduced by the choice of supersymmetric parameters which govern the radiative corrections. In the so-called maximal mixing scenario where $A_t^2 = 6M_{\text{SUSY}}^2$, the approximate expression for $\delta\mathcal{M}_{12}^2$ vanishes. For large values of $\tan\beta$, the measured Higgs mass, $m_h \sim 125$ GeV is not compatible with the maximal mixing scenario as defined in Ref. [78], so it is reasonable to take $6 - X_t A_t/M_{\text{SUSY}}^2 \sim \mathcal{O}(1)$. As an example, for $\tan\beta \gg 1$, $A_t \sim 2M_{\text{SUSY}}$ and $\mu \sim -2M_{\text{SUSY}}$, one finds numerically that

$$\cos(\beta - \alpha) \sim \left(\frac{28 \text{ GeV}}{m_A}\right)^2. \qquad \text{(B14)}$$

Choosing extreme parameters, $\tan\beta = 50$ and $\Delta_b = -0.5$, we see that it is just possible to achieve a value of $vg_{hb\bar{b}}/m_b$ close to -1 if $m_A = 200$ GeV. However, this value of m_A is uncomfortably close to m_Z and m_h, in which case one must check that terms of $\mathcal{O}(m_Z^2/m_A^2)$, which have been neglected in the above analysis, do not spoil the estimate. Increasing the magnitude of μ or taking A_t slightly above its maximal mixing value would allow for a wrong-sign $hb\bar{b}$ coupling together with a somewhat higher value of m_A.

Similar considerations also apply to the $h\tau^+\tau^-$ coupling. However, the expression for Δ_τ [analogous to Eq. (B8) for Δ_b] involves only terms proportional to electroweak gauge couplings. Hence, the effects of Δ_τ only have a small impact on $g_{h\tau^+\tau^-}$. Thus, it is even harder to find a sensible parameter regime in which $vg_{h\tau^+\tau^-}/m_\tau$ is close to -1. We conclude that in the MSSM, the wrong-sign $hb\bar{b}$ and $h\tau^+\tau^-$ couplings are not possible for generic choices of the MSSM parameters. Nevertheless, based on an approximate

treatment of the leading radiative corrections, it seems that some extreme regions of the parameter space do exist in which a value of $vg_{hb\bar{b}}/m_b$ close to -1 can be achieved due to large radiative correction effects in the large $\tan\beta$ regime. A more detailed study of the MSSM Higgs parameter space based on a more complete analysis of the radiative corrections lies beyond the scope of this paper.

APPENDIX C: NONDECOUPLING OF THE $H^\pm$ LOOP CONTRIBUTION TO THE $h \to \gamma\gamma$ AMPLITUDE AND THE $\kappa_D < 0$ SCENARIO

In this appendix, we give a detailed treatment of the nondecoupling of the $H^\pm$ loop contribution to the $h \to \gamma\gamma$ amplitude discussed at the end of Sec. III, focusing on its impact on the wrong-sign Yukawa coupling scenario, i.e. $\kappa_D < 0$. In particular, we demonstrate that the

charged-Higgs contribution to the $h\gamma\gamma$ coupling in the $\kappa_D < 0$ case is approximately constant and *always* sufficiently significant as to eventually be observable at the LHC. In addition, we display explicitly the constraints coming from tree-level unitarity, which imply that the $\kappa_D < 0$ scenario is only perturbatively reliable for $m_{H^\pm} \lesssim 650$ GeV. We also remark on nondecoupling of the charged-Higgs loop for some $\kappa_D > 0$ scenarios.[12]

To begin, let us first recall the basic formulae from Ref. [16] in the case of $\lambda_6 = \lambda_7 = 0$ considered in this paper, as summarized in Sec. III. The crucial ingredients are the mass-squared relation of Eq. (3.28) and the expression Eq. (3.27) for the hH^+H^- coupling, $G_{hH^+H^-}$ [cf. Eq. (C7)]. For the purposes of this appendix, it is useful to rearrange some of the angular factors and to define the dimensionless coupling

$$g_{hH^+H^-} \equiv \frac{G_{hH^+H^-}}{v} = \frac{(2m_A^2 - 2m_{H^\pm}^2 - m_h^2)\sin(\beta - \alpha)\sin\beta\cos\beta + (m_A^2 - m_h^2)\cos 2\beta\cos(\beta - \alpha) + \lambda_5 v^2 \cos(\beta + \alpha)}{v^2 \sin\beta\cos\beta}. \quad \text{(C1)}$$

In the decoupling limit described in Sec. III, we have $\sin(\beta - \alpha) \to 1$, $\cos(\beta - \alpha) \to 0$, and $m_A^2 \sim m_H^2 \sim m_{H^\pm}^2 \gg v^2$. The first term inside the brackets of Eq. (C1) is of order v^2 because of the mass relations (keeping the λ_i perturbative) and the second term is of order v^2 because $\cos(\beta - \alpha) \propto v^2/m_A^2$. To discuss the third term we need to note that for $\sin(\beta - \alpha) \to 1$ we have $\alpha \to \beta - \pi/2$. Then, the third term approaches $2v^2\lambda_5$ since $\cos(\beta + \alpha) \to \sin 2\beta = 2\sin\beta\cos\beta$. The net result is that $g_{hH^+H^-}$ is not growing with the Higgs mass squared and so the charged-Higgs loop contribution to the $h \to \gamma\gamma$ amplitude is suppressed by a factor of $m_W^2/m_{H^\pm}^2$ relative to the W and t and b loops. This is in correspondence with the idea that any heavy particle that does not acquire mass from the Higgs vacuum expectation value should decouple.

However, the situation is *necessarily* quite different in the case of $\kappa_D < 0$, where $\sin(\beta + \alpha) \to 1$, implying $\alpha \to \pi/2 - \beta$. In this limit, $\cos(\beta - \alpha) \to \sin 2\beta$ so that the second term in the numerator of Eq. (C1) is approximated by $2(m_A^2 - m_h^2)\cos 2\beta$ which approaches $\sim 2m_{H^\pm}^2 \cos 2\beta$ as $m_A^2 \sim m_H^2 \sim m_{H^\pm}^2 \to \infty$ (at fixed $m_h \sim 125$ GeV). Of course, if $\tan\beta$ is large then $\cos 2\beta \to -1$. Thus, we see from Eq. (C1) that for $\kappa_D < 0$ we have

$$\frac{v^2 g_{hH^+H^-}}{m_{H^\pm}^2} \sim -2, \quad \text{(C2)}$$

implying that the $H^\pm$ loop contribution to the $h \to \gamma\gamma$ amplitude will never decouple. In practice, Eq. (C2) implies that the modification cannot be detected if the $\mu_f^h(\text{LHC})$ values are only measured to be within 20% or 10% of unity, whereas no $\kappa_D < 0$ points survive if the $\mu_f^h(\text{LHC})$ values are found to be within 5% of unity, as illustrated in Fig. 9. In contrast, the range of allowed values of $v^2 g_{hH^+H^-}/m_{H^\pm}^2$ in the case of $\kappa_D > 0$ is much larger, from nondecoupling values of $\mathcal{O}(1)$ (both positive and negative) to decoupling values significantly less than 1. Note that the results of Fig. 9 indicate that, as in the $\kappa_D < 0$ scenario, the points in the case of $\kappa_D > 0$ with $v^2 g_{hH^+H^-}/m_{H^\pm}^2 \lesssim -2$ will not survive if all the $\mu_f^h(\text{LHC})$ are measured to be within 5% of the SM value of unity.
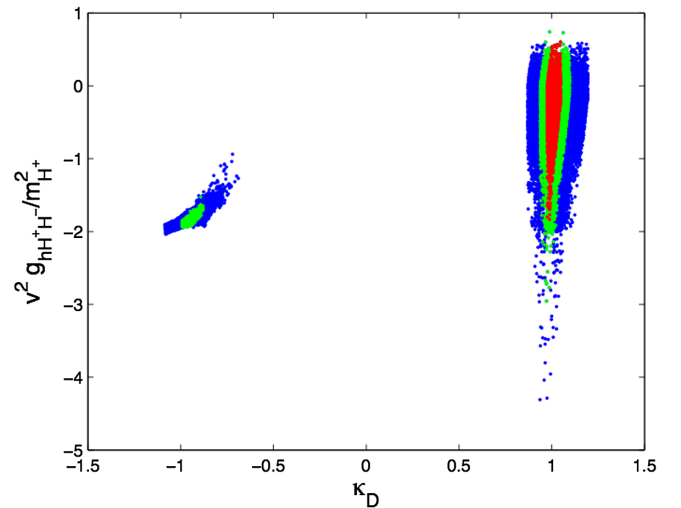

FIG. 9 (color online). We show points in the $v^2 g_{hH^+H^-}/m_{H^\pm}^2$ vs κ_D plane with the standard color scheme of Fig. 2.
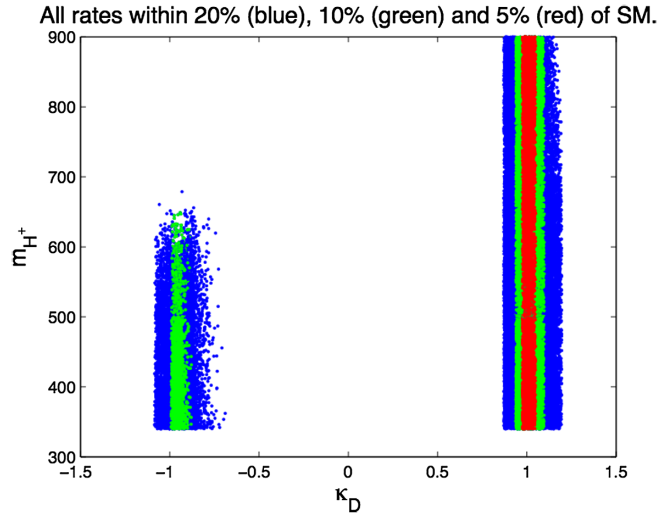
---

[12]The phenomenological effects of the nondecoupling charged-Higgs loop contribution to the $h \to \gamma\gamma$ amplitude and other 2HDM observables have also been considered in Refs. [58] and [59].

FIG. 10 (color online). We show points in the $m_{H^\pm}$ vs κ_D plane with the standard color scheme of Fig. 2. Note: 900 GeV is the largest $m_{H^\pm}$ considered in the scans—the $\kappa_D \sim +1$ region would extend to arbitrarily large $m_{H^\pm}$ corresponding to the decoupling limit.

We have already noted that in the $\kappa_D < 0$ scenario there will be a limitation on $m_{H^\pm}^2$ coming from perturbativity and unitarity. The relevant constraints are incorporated in all of our plots. Once $m_{H^\pm}$ becomes too large, the theory becomes perturbatively unreliable and insisting on tree-level unitarity will then imply that only the $\kappa_D > 0$ possibility is allowed. So, in this sense, nondecoupling is only possible temporarily for an intermediate range of heavy $H^\pm$ masses if we insist that $m_{H^\pm}$ not be so large that the tree-level unitarity bound is violated. In order to illustrate the nature of the unitarity limits, we present some plots.

In Fig. 10, we show points in the $m_{H^\pm}$ vs κ_D plane allowed when all the $\mu_f^h(\text{LHC})$s are within 20%, 10% or 5%

of unity. We see clearly that $m_{H^\pm}$ is limited to lie below about 650 GeV in the $\kappa_D < 0$ case while it can be arbitrarily large (we only scan up to 900 GeV) for the standard $\kappa_D > 0$ scenario that allows for true decoupling. We have found that the maximum $m_{H^\pm}$ value is limited by the tree-level unitarity limits of the λ_i, in particular λ_3. In Fig. 11, we display in the left panel λ_3 as a function of κ_D for both the $\kappa_D > 0$ and $\kappa_D < 0$ scenarios; and in the right panel we show $|\lambda_3|$ as a function of $m_{H^\pm}$ for the $\kappa_D < 0$ and $\kappa_D > 0$ scenarios requiring only that all $\mu_f^h(\text{LHC})$'s be within 20% of unity. Given that the tree-level unitarity bounds on the λ_i are of order $|\lambda_i| \lesssim 15$, we see that it is λ_3 that encounters this upper limit at large $m_{H^\pm}$ in the $\kappa_D < 0$ case, whereas it is clear that in the $\kappa_D > 0$ case arbitrarily large $m_{H^\pm}$ is possible without violating tree-level unitarity bounds, consistent with the decoupling limit. However, one should also note the significant number of $\kappa_D > 0$ points that hit the tree-level unitarity bound for which nondecoupling is again possible.

The actual limits based on tree-level unitarity bounds are imposed in terms of various λ_i amplitude combinations, of which it is

$$a^+ = \frac{1}{16\pi} \left[\frac{3}{2} (\lambda_1 + \lambda_3) + \sqrt{\frac{9}{4} (\lambda_1 - \lambda_2)^2 + (2\lambda_3 + \lambda_4)^2} \right]$$

(C3)

that is most constraining. In Fig. 12 we plot $|a^+|$ as a function of κ_D and of $m_{H^\pm}$ using the same format as in Fig. 11. Note that $|a^+|$ is hitting the tree-level unitarity bound of 0.5 for both the $\kappa_D < 0$ and $\kappa_D > 0$ scenarios. However, there is no limit on the associated $m_{H^\pm}$ value in the latter case, whereas there is the already quoted limit of ~ 650 GeV in the former case.

We now show that for the type-II 2HDM with $\kappa_D < 0$, where $v^2 g_{hH^+H^-}/m_{H^\pm} \sim -2$, and with $\kappa_D > 0$, where
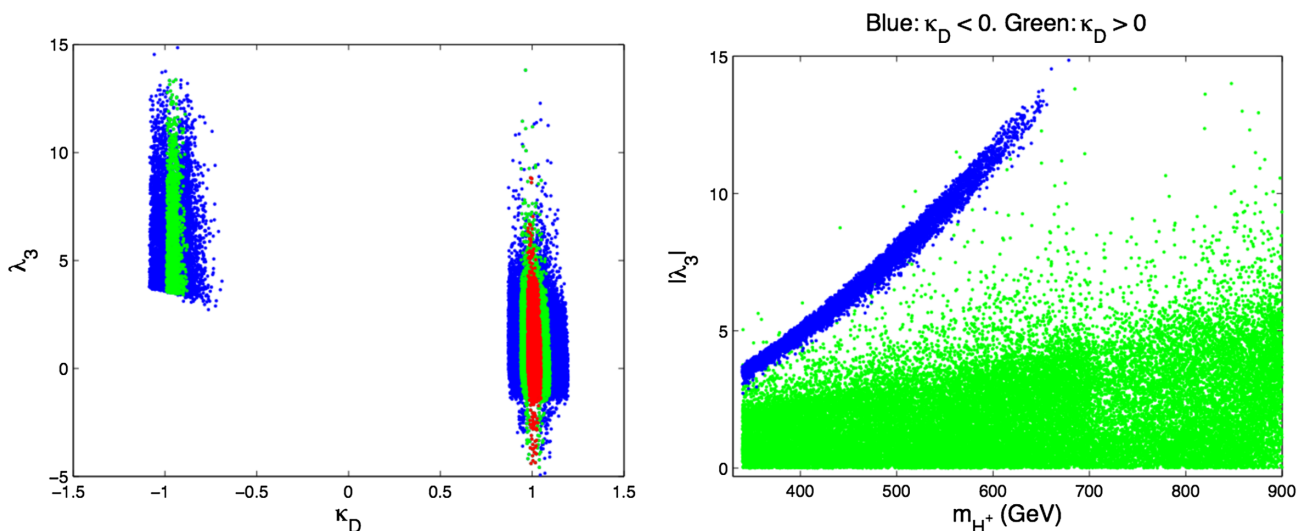

FIG. 11 (color online). In the left panel we plot λ_3 vs κ_D using the color scheme of Fig. 2; in the right panel we plot $|\lambda_3|$ vs $m_{H^\pm}$ for $\kappa_D < 0$ (blue/black) and $\kappa_D > 0$ (green/light gray) points with all $\mu_f^h(\text{LHC})$ within 20% of unity.
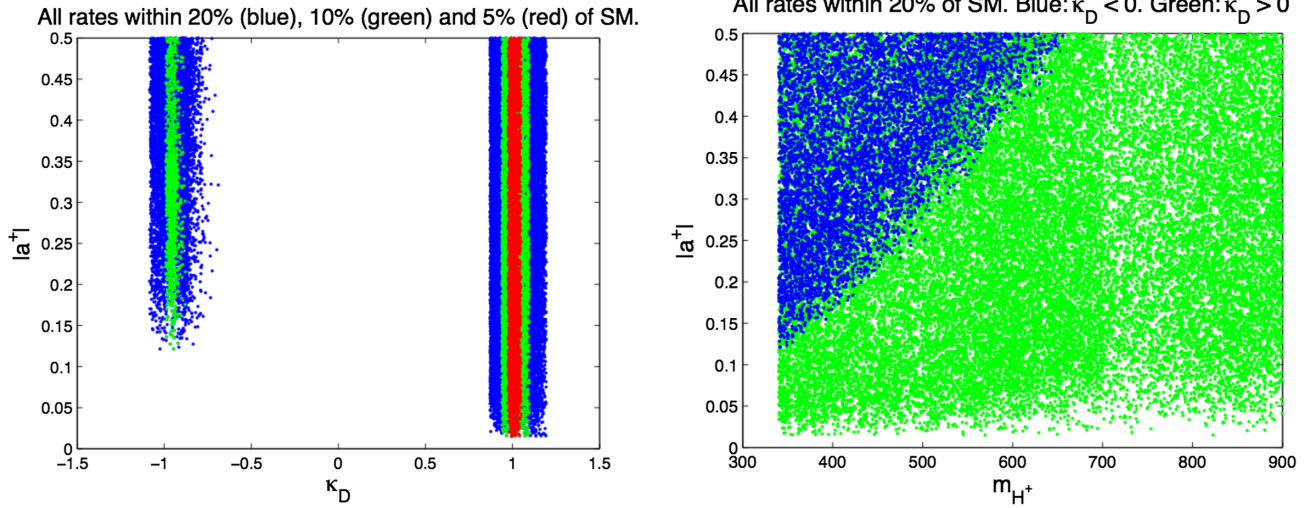
FIG. 12 (color online). In the left panel we plot $|a^+|$ vs κ_D using the color scheme of Fig. 2; in the right panel we plot $|a^+|$ vs $m_{H^\pm}$ for $\kappa_D < 0$ (blue/black) and $\kappa_D > 0$ (green/light gray) points with all $\mu_f^h(\text{LHC})$ within 20% of unity.

$v^2 g_{hH^+H^-}/m_{H^\pm} \lesssim -2$ (cf. Fig. 9), the loop functions are such that the charged-Higgs loop contributes with the same sign as the top-quark loop and thus will reduce the $h \to \gamma\gamma$ width, both canceling part of the W-loop contribution of the opposite sign. As we have seen earlier, and will show numerically below, we find that this reduction is sufficient to prevent the $\gamma\gamma$ channel from ever approaching the SM prediction and by an amount that will be seen at the LHC with high luminosity.

Let us now give more details. We will employ a simplified version of the notation of CPSUPERH [79]. One finds

$$\Gamma(h \to \gamma\gamma) = \frac{\alpha^2 g^2}{256\pi^3} \frac{m_h^3}{v^2} |S|^2, \tag{C4}$$

where[13]

$$
\begin{aligned}
S &= 2\sum_{f=b,t}\left[N_c q_f^2 g_f g_{hf\bar{f}} \frac{v}{m_f} F_{1/2}(\tau_f) - g_{hWW} F_1(\tau_W) - g_{hH^+H^-} \frac{v^2}{2m_{H^\pm}^2} F_0(\tau_{H^\pm})\right] \\
&\equiv 2\sum_f [S_f^h F_{1/2}(\tau_f) + S_W^h F_1(\tau_W) + S_{H^\pm}^h F_0(\tau_{H^\pm})] \\
&\equiv \sum_f (I_f^h + I_W^h + I_{H^\pm}^h),
\end{aligned}
\tag{C5}
$$

where $\tau_i = m_h^2/(4m_i^2)$, $N_c = 3$, and the various F's are

$$
\begin{aligned}
F_{1/2}(\tau) &= \tau^{-1}[1 + (1 - \tau^{-1})f(\tau)], \\
F_1(\tau) &= 2 + 3\tau^{-1} + 3\tau^{-1}(2 - \tau^{-1})f(\tau), \\
F_0(\tau) &= \tau^{-1}[-1 + \tau^{-1}f(\tau)].
\end{aligned}
\tag{C6}
$$

The function $f(\tau)$ is that defined in Eq. (40) of Ref. [79]. In the $\tau \to 0$ limit, $F_{1/2} \to 2/3$, $F_1 \to 7$ and $F_0 \to 1/3$. In Eq. (C5), $g_f = gm_f/(2m_W)$ and the other g's are defined by the interaction Lagrangians,

$$
\begin{aligned}
\mathcal{L}_{hWW} &= (gm_W)g_{hWW}W^+_{\ \mu}W^{-\mu}h, \\
\mathcal{L}_{hf\bar{f}} &= -\frac{gm_f}{2m_W}g_{hf\bar{f}}h\bar{f}f, \\
\mathcal{L}_{hH^+H^-} &= vg_{hH^+H^-}hH^+H^-,
\end{aligned}
\tag{C7}
$$

where $g_{hH^+H^-} \equiv G_{hH^+H^-}/v$ as defined in Eq. (C1).

In the $\kappa_D > 0$ case with $\sin(\beta - \alpha) \to 1$ we have $\alpha \to \beta - \pi/2$, for which $\cos(\beta - \alpha) \propto v^2/m_A^2$, $\sin\alpha \to -\cos\beta$ and $\cos\alpha \to \sin\beta$ with the result

$$S_{u,c,t}^h \to 1, \qquad S_{d,s,b,e,\mu,\tau}^h \to +1,$$

$$S_W^h = -\sin(\beta - \alpha) \to -1, \qquad S_{H^\pm}^h \propto \frac{v^2}{m_W^2}. \tag{C8}$$

---

[13]Relative to Ref. [13], the $F_{1/2}$ defined here is one-half as large and F_0 has the opposite sign.

In the $\kappa_D < 0$ case we have $\alpha \to \pi/2 - \beta$, for which $\sin\alpha \to \cos\beta$, $\cos\alpha \to \sin\beta$, $\cos(\beta - \alpha) \to \sin(2\beta)$, and $\sin(\beta - \alpha) \to -\cos(2\beta) = (\tan^2\beta - 1)/(\tan^2\beta + 1)$. For simplicity, consider $\tan\beta \to \infty$ and the limit of large $m_A^2 \sim m_{H^\pm}^2$. We then have

$$S_{u,c,t}^h \to 1, S_{d,s,b,e,\mu,\tau}^h \to -1,$$
$$S_W^h = -\sin(\beta - \alpha) \to -1, S_{H^\pm}^h \to 1. \qquad (C9)$$

The important thing to note here is that the $H^\pm$ loop contributes with the same sign as the top loop, i.e. it too will cancel against the negative W loop and decrease the $h \to \gamma\gamma$ width.

In more detail, we have the following. For both $\kappa_D > 0$ and $\kappa_D < 0$, the relative contributions of the top-quark loop and the W loop to S are $I_W^h \simeq -8.3233$ and $I_t^h = +1.8351$. As regards the charged-Higgs loop, for $\kappa_D < 0$ and large $m_{H^\pm}$ one gets $I_{H^\pm}^h = +0.33333$. As regards the b-quark loop, for the case of $\kappa_D > 0$ we have $I_b^h = -0.0279 + 0.04i$. Of course, this changes sign for $\kappa_D < 0$. We will neglect other quarks and leptons for simplicity since their contributions are quite small.

Then, in the SM $\kappa_D > 0$ case, neglecting the decoupled charged-Higgs loops, we find $\sum_{i=W,t,b} I_i^h = -6.5161 + 0.04i$. If we consider the $\kappa_D < 0$ case without including the charged-Higgs loop one finds $\sum_{i=W,t,b} I_i^h = -6.4603 - 0.04i$. The ratio of the absolute values is 0.99, a less than 1% decrease in κ_γ and certainly not measurable at the LHC. However, after including the charged-Higgs loop we obtain $\sum_{i=W,t,b,H^\pm} I_i^h = -6.127 - 0.04i$ with the charged-Higgs loop evaluated at large $m_{H^\pm}$, which translates to $\kappa_\gamma \sim 0.94$ corresponding to a 12% decrease in $\Gamma(h \to \gamma\gamma)$. In fact, this level of decrease is very characteristic of the full scan as shown in Fig. 9 and is measurable at the LHC with $\sqrt{s} = 14$ TeV and $L \geq 300$ fb^{-1}. As already noted, this same level of decrease also occurs for those $\kappa_D > 0$ scenarios for which the charged-Higgs loop does not decouple, i.e. roughly if $v^2 g_{hH^+H^-}/m_{H^\pm} \lesssim -2$ (see Fig. 9).

Of course, in the computations presented in the main text, the full set of quarks and leptons is included, the charged-Higgs mass is varied as part of the scan (with the lower bound of 340 GeV) and current LHC Higgs constraints are imposed as well as constraints from perturbativity, unitarity and precision electroweak measurements. As we have said above, all this leads to only small numerical changes relative to the κ_γ decrease for $\kappa_D < 0$ quoted above; thus, the nondecoupling of the $H^\pm$ loop for $\kappa_D < 0$ leads to a decrease in κ_γ that is at least as large as 5%.

[1] G. Aad *et al.* (ATLAS Collaboration), Phys. Lett. B **716**, 1 (2012).

[2] S. Chatrchyan *et al.* (CMS Collaboration), Phys. Lett. B **716**, 30 (2012).

[3] G. Aad *et al.* (ATLAS Collaboration), Phys. Lett. B **726**, 88 (2013).

[4] S. Chatrchyan *et al.* (CMS Collaboration), Phys. Rev. D **89**, 092007 (2014).

[5] M. Carena, C. Grojean, M. Kado, and V. Sharma, http://pdg.lbl.gov/2013/reviews/rpp2013-rev-higgs-boson.pdf, to appear in the 2014 edition of the Review of Particle Physics by the Particle Data Group.

[6] J. R. Espinosa, C. Grojean, M. Mühlleitner and M. Trott, J. High Energy Phys. 12 (2012) 045.

[7] A. Falkowski, F. Riva, and A. Urbano, J. High Energy Phys. 11 (2013) 111.

[8] G. Belanger, B. Dumont, U. Ellwanger, J. F. Gunion, and S. Kraml, Phys. Rev. D **88**, 075008 (2013).

[9] A. Celis, V. Ilisie and A. Pich, J. High Energy Phys. 12 (2013) 095.

[10] P. M. Ferreira, R. Santos, M. Sher, and J. P. Silva, Phys. Rev. D **85**, 077703 (2012); D. Carmi, A. Falkowski, E. Kuflik, and T. Volansky, J. High Energy Phys. 07 (2012) 136; H. S. Cheon and S. K. Kang, J. High Energy Phys. 09 (2013) 085; W. Altmannshofer, S. Gori, and G. D. Kribs, Phys. Rev. D **86**, 115009 (2012); Y. Bai, V. Barger, L. L. Everett, and G. Shaughnessy, Phys. Rev. D **87**, 115013 (2013); C.-Y. Chen and S. Dawson, Phys. Rev. D **87**, 055016 (2013); A. Celis, V. Ilisie, and A. Pich, J. High Energy Phys. 07 (2013) 053; C-W. Chiang and K. Yagyu, J. High Energy Phys. 07 (2013) 160; M. Krawczyk, D. Sokolowska, and B. Swiezewska, J. Phys. Conf. Ser. **447**, 012050 (2013); B. Grinstein and P. Uttayarat, J. High Energy Phys. 06 (2013) 094; 09 (2013) 110(E); A. Barroso, P. M. Ferreira, R. Santos, M. Sher, and J. P. Silva, arXiv:1304.5225; B. Coleppa, F. Kling, and S. Su, J. High Energy Phys. 01 (2014) 161; P. M. Ferreira, R. Santos, M. Sher, and J. P. Silva, arXiv:1305.4587; O. Eberhardt, U. Nierste, and M. Wiebusch, J. High Energy Phys. 07 (2013) 118; S. Choi, S. Jung, and P. Ko, J. High Energy Phys. 10 (2013) 225; V. Barger, L. L. Everett, H. E. Logan, and G. Shaughnessy, Phys. Rev. D **88**, 115003 (2013); D. López-Val, T. Plehn, and M. Rauch, J. High Energy Phys. 10 (2013) 134; S. Chang, S. K. Kang, J.-P. Lee, K. Y. Lee, S. C. Park, and J. Song, arXiv:1310.3374; G. Cacciapaglia, A. Deandrea, G. D. La Rochelle, and J.-B. Flament, arXiv:1311.5132; K. Cranmer, S. Kreiss, D. López-Val, and T. Plehn, arXiv:1401.0080.

[11] K. Inoue, A. Kakuto, H. Komatsu, and S. Takeshita, Prog. Theor. Phys. **67**, 1889 (1982); R. A. Flores and M. Sher, Ann. Phys. (N.Y.) **148**, 95 (1983); J. F.

Gunion and H. E. Haber, Nucl. Phys. **B272**, 1 (1986); **B402**, 567(E) (1993); **B278**, 449 (1986); **B402**, 569(E) (1993).

[12] T. D. Lee, Phys. Rev. D **8**, 1226 (1973).

[13] J. F. Gunion, H. E. Haber, G. L. Kane, and S. Dawson, *The Higgs Hunter's Guide* (Westview Press, Boulder, CO, 2000).

[14] G. C. Branco, P. M. Ferreira, L. Lavoura, M. N. Rebelo, M. Sher, and J. P. Silva, Phys. Rep. **516**, 1 (2012).

[15] S. L. Glashow and S. Weinberg, Phys. Rev. D **15**, 1958 (1977); E. A. Paschos, Phys. Rev. D **15**, 1966 (1977).

[16] J. F. Gunion and H. E. Haber, Phys. Rev. D **67**, 075019 (2003).

[17] P. M. Ferreira, R. Santos, and A. Barroso, Phys. Lett. B **603**, 219 (2004); **629**, 114(E) (2005).

[18] H. E. Haber, G. L. Kane, and T. Sterling, Nucl. Phys. **B161**, 493 (1979).

[19] L. J. Hall and M. B. Wise, Nucl. Phys. **B187**, 397 (1981).

[20] J. F. Donoghue and L. F. Li, Phys. Rev. D **19**, 945 (1979).

[21] A. Arhrib, P. M. Ferreira and R. Santos, J. High Energy Phys. 03 (2014) 053.

[22] N. G. Deshpande and E. Ma, Phys. Rev. D **18**, 2574 (1978).

[23] S. Kanemura, T. Kubota, and E. Takasugi, Phys. Lett. B **313**, 155 (1993); A. G. Akeroyd, A. Arhrib, and E. M. Naimi, Phys. Lett. B **490**, 119 (2000).

[24] M. E. Peskin and T. Takeuchi, Phys. Rev. D **46**, 381 (1992).

[25] C. D. Froggatt, R. G. Moorhouse, and I. G. Knowles, Phys. Rev. D **45**, 2471 (1992); W. Grimus, L. Lavoura, O. M. Ogreid, and P. Osland, Nucl. Phys. **B801**, 81 (2008); H. E. Haber and D. O'Neil, Phys. Rev. D **83**, 055017 (2011).

[26] The ALEPH, CDF, D0, DELPHI, L3, OPAL, SLD Collaborations, the LEP Electroweak Working Group, the Tevatron Electroweak Working Group, and the SLD Electroweak and Heavy Flavour Groups, arXiv:1012.2367.

[27] M. Baak, M. Goebel, J. Haller, A. Hoecker, D. Ludwig, K. Moenig, M. Schott, and J. Stelzer, Eur. Phys. J. C **72**, 2003 (2012).

[28] M. Baak, M. Goebel, J. Haller, A. Hoecker, D. Kennedy, R. Kogler, K. Moenig, M. Schott, and J. Stelzer, Eur. Phys. J. C **72**, 2205 (2012).

[29] A. Barroso, P. M. Ferreira, I. P. Ivanov, and R. Santos, J. High Energy Phys. 06 (2013) 045.

[30] T. Hermann, M. Misiak, and M. Steinhauser, J. High Energy Phys. 11 (2012) 036; M. Misiak, H. M. Asatrian, K. Bieri, M. Czakon, A. Czarnecki, T. Ewerth, A. Ferroglia, P. Gambino *et al.*, Phys. Rev. Lett. **98**, 022002 (2007); D. Asner *et al.* (Heavy Flavor Averaging Group Collaboration), arXiv:1010.1589.

[31] F. Mahmoudi and O. Stal, Phys. Rev. D **81**, 035016 (2010); S. Su and B. Thomas, Phys. Rev. D **79**, 095014 (2009); M. Aoki, S. Kanemura, K. Tsumura, and K. Yagyu, Phys. Rev. D **80**, 015017 (2009); P. Posch, Ph.D. dissertation, University of Vienna, 2009.

[32] A. Freitas and Y.-C. Huang, J. High Energy Phys. 08 (2012) 050; 05 (2013) 074(E); 10 (2013) 044(E).

[33] A. Denner, R. J. Guth, W. Hollik, and J. H. Kuhn, Z. Phys. C **51**, 695 (1991).

[34] M. Boulware and D. Finnell, Phys. Rev. D **44**, 2054 (1991).

[35] A. K. Grant, Phys. Rev. D **51**, 207 (1995).

[36] H. E. Haber and H. E. Logan, Phys. Rev. D **62**, 015011 (2000).

[37] G. Abbiendi *et al.* (ALEPH, DELPHI, L3, OPAL, and LEP Collaborations), Eur. Phys. J. C **73**, 2463 (2013).

[38] ATLAS Collaboration, Report No. ATLAS-CONF-2013-090; G. Aad *et al.* (ATLAS Collaboration), J. High Energy Phys. 06 (2012) 039.

[39] S. Chatrchyan *et al.* (CMS Collaboration), J. High Energy Phys. 07 (2012) 143.

[40] J. P. Lees *et al.* (*BABAR* Collaboration), Phys. Rev. Lett. **109**, 101802 (2012).

[41] J. F. Donoghue and L. F. Li, Phys. Rev. D **19**, 945 (1979).

[42] H. Georgi and D. V. Nanopoulos, Phys. Lett. **82B**, 95 (1979).

[43] F. J. Botella and J. P. Silva, Phys. Rev. D **51**, 3870 (1995).

[44] L. Lavoura and J. P. Silva, Phys. Rev. D **50**, 4619 (1994).

[45] L. Lavoura, Phys. Rev. D **50**, 7089 (1994).

[46] G. C. Branco, L. Lavoura, and J. P. Silva, *CP Violation* (Oxford University Press, Oxford, 1999), Chap. 22.

[47] S. Davidson and H. E. Haber, Phys. Rev. D **72**, 035004 (2005); **72** 099902(E) (2005).

[48] H. E. Haber and Y. Nir, Nucl. Phys. **B335**, 363 (1990).

[49] M. Carena, H. E. Haber, H. E. Logan, and S. Mrenna, Phys. Rev. D **65**, 055005 (2002); **65**, 099902(E) (2002).

[50] N. Craig, J. Galloway, and S. Thomas, arXiv:1305.2424.

[51] D. M. Asner, T. Barklow, C. Calancha, K. Fujii, N. Graf, H. E. Haber, A. Ishikawa, S. Kanemura *et al.*, arXiv:1310.0763.

[52] M. Carena, I. Low, N. R. Shah, and C. E. M. Wagner, J. High Energy Phys. 04 (2014) 015.

[53] H. E. Haber, arXiv:1401.0152.

[54] H. E. Haber, M. J. Herrero, H. E. Logan, S. Penaranda, S. Rigolin, and D. Temes, Phys. Rev. D **63**, 055004 (2001).

[55] I. F. Ginzburg, M. Krawczyk, and P. Osland, LC Note No. LC-TH-2001-026; Nucl. Instrum. Methods Phys. Res., Sect. A **472**, 149 (2001); in *Physics and Experiments with Future Linear e^+e^- Colliders*, AIP Conf. Proc. No. 578 (AIP, New York, 2001), pp. 304–311.

[56] I. F. Ginzburg and M. Krawczyk, Phys. Rev. D **72**, 115013 (2005).

[57] A. Arhrib, R. Benbrik, and C.-W. Chiang, Phys. Rev. D **77**, 115013 (2008).

[58] A. Arhrib, M. Capdequi Peyranere, W. Hollik, and S. Penaranda, Phys. Lett. B **579**, 361 (2004).

[59] G. Bhattacharyya, D. Das, P. B. Pal, and M. N. Rebelo, J. High Energy Phys. 10 (2013) 081.

[60] A. David *et al.* (LHC Higgs Cross Section Working Group Collaboration), arXiv:1209.0040.

[61] S. Dawson, A. Gritsan, H. Logan, J. Qian, C. Tully, R. Van Kooten *et al.*, arXiv:1310.8361.

[62] H. Ono and A. Miyamoto, Eur. Phys. J. C **73**, 2343 (2013).

[63] https://twiki.cern.ch/twiki/bin/view/LHCPhysics/CrossSectionsFigures#Higgs_production_cross_sections.

[64] R. V. Harlander and W. B. Kilgore, Phys. Rev. D **68**, 013001 (2003).

[65] M. Spira, arXiv:hep-ph/9510347.

[66] B. Dumont, J. F. Gunion, Y. Jiang, and S. Kraml, arXiv:1405.3584.

[67] A. Djouadi, J. Kalinowski, and M. Spira, Comput. Phys. Commun. **108**, 56 (1998).

[68] R. Harlander, M. Mühlleitner, J. Rathsman, M. Spira, and O. Stål, arXiv:1312.5571.

[69] D. Eriksson, J. Rathsman, and O. Stål, Comput. Phys. Commun. **181**, 189 (2010).

[70] H. E. Haber and D. O'Neil, Phys. Rev. D **74**, 015018 (2006); **74**, 059905(E) (2006).

[71] M. Carena and H. E. Haber, Prog. Part. Nucl. Phys. **50**, 63 (2003).

[72] A. Djouadi, Phys. Rep. **459**, 1 (2008).

[73] H. E. Haber and R. Hempfling, Phys. Rev. Lett. **66**, 1815 (1991); J. R. Ellis, G. Ridolf,i and F. Zwirner, Phys. Lett. B **257**, 83 (1991); Y. Okada, M. Yamaguchi, and T. Yanagida, Prog. Theor. Phys. **85**, 1 (1991).

[74] H. E. Haber and R. Hempfling, Phys. Rev. D **48**, 4280 (1993).

[75] H. E. Haber and J. D. Mason, Phys. Rev. D **77**, 115011 (2008).

[76] M. Carena, D. Garcia, U. Nierste, and C. E. M. Wagner, Nucl. Phys. **B577**, 88 (2000).

[77] R. Hempfling, Phys. Rev. D **49**, 6168 (1994); L. J. Hall, R. Rattazzi, and U. Sarid, Phys. Rev. D **50**, 7048 (1994); M. Carena, M. Olechowski, S. Pokorski, and C. E. M. Wagner, Nucl. Phys. **B426**, 269 (1994); D. M. Pierce, J. A. Bagger, K. T. Matchev, and R.-J. Zhang, Nucl. Phys. **B491**, 3 (1997).

[78] M. Carena, S. Heinemeyer, O. Stål, C. E. M. Wagner, and G. Weiglein, Eur. Phys. J. C **73**, 2552 (2013).

[79] J. S. Lee, A. Pilaftsis, M. Carena, S. Y. Choi, M. Drees, J. R. Ellis, and C. E. M. Wagner, Comput. Phys. Commun. **156**, 283 (2004).